

## SUPPLEMENT 1

## Table of Contents

## 1. Methods

- a. *Study Design*
  - b. *Metabarcoding Collection Isolation, Amplification, and Sequencing*
  - c. *Bioinformatics*
  - d. *Microscopy Identification of Ichthyoplankton*
  - e. *Estimating Abundance (see Supplement 2)*
  - f. *Environmental Covariates*
  - g. *Data analysis*

## **2. Results**

- a. Change in Fish Assemblage Structure over Time
  - b. Metabarcoding Signal Does Not Degrade Over Time

### **3. Figures**

- a. *Figure S1. station Map*
  - b. *Figure S2. Observed Sequence Reads vs. Observed Morphological Counts*
  - c. *Figure S3. Predicted Counts vs. Observed Morphological Counts*
  - d. *Figure S4. Predicted Sequence Reads vs. Observed Sequence Reads*
  - e. *Figure S5. Co-detection of Taxa By Metabarcoding and Microscopy*
  - f. *Figure S6. Temperature Associations in Fish Species*
  - g. *Figure S7. Southern Oceanic Species Drive Fish Community Shifts*
  - h. *Figure S8. Significant Species Occurrence and SST Correlations at each Station*

- 23           i. *Figure S9. Significant Species Occurrence and MWCT Correlations at each*  
24           *Station*
- 25           j. *Figure S10. Significant Species Abundance and SST Correlations at each station*
- 26           k. *Figure S11. Significant Species Abundance and MWCT Correlations at each*  
27           *station*
- 28           l. *Figure S12. Bar Plot of Significant Species Abundance and SST Correlations*  
29           *Across All stations*
- 30           m. *Figure S13. Bar Plot of Significant Species Abundance and MWCT Correlations*  
31           *Across All stations*
- 32           n. *Figure S14. Increased Abundance of Southern Mesopelagic Species with Higher*  
33           *SST*
- 34           o. *Figure S15. Increased Abundance of Southern and Central Mesopelagic Species*  
35           *with Higher SST*
- 36           p. *Figure S16. Heat Map of Abundances Over Time*
- 37           q. *Figure S17. NMDS Ordination of Species and Years*
- 38           r. *Figure S18. NMDS Ordination of Species and Samples*
- 39           s. *Figure S19. Heat Map of San Diego Offshore Abundances Over Time*
- 40           t. *Figure S20. NMDS Ordination of San Diego Offshore Species and Years*
- 41           u. *Figure S21. Heat Map of San Diego Inshore Abundances Over Time*
- 42           v. *Figure S22. NMDS Ordination of San Diego Inshore Species and Years*
- 43           w. *Figure S23. Heat Map of Pt. Conception Abundances Over Time*
- 44           x. *Figure S24. NMDS Ordination of Pt. Conception Species and Years*
- 45           y. *Figure S25. Heat Map of San Nicholas Island Abundances Over Time*

46           z. *Figure S26. NMDS Ordination of San Nicholas Island Species and Years*  
47           aa. *Figure S27. Co-occurrence Patterns of Species Controlling for SST*  
48           bb. *Figure S28. Co-occurrence Patterns of Species*  
49           cc. *Figure S39. Differential Species Abundance Before and After the Marine Heat*  
50           *Wave at the San Nicholas Island*  
51           dd. *Figure S30. Stable Precision of Amplicon Abundance Over Time*  
52           ee. *Figure S31. Stable Precision of Abundance Estimates Over Time*  
53

## 54       **Introduction**

55           This supplemental material provides additional details on the methods, results, and  
56           discussion to support the main findings and conclusion of the manuscript.

57           The CalCOFI program (<https://calcofi.com/>) serves to provide fisheries-independent  
58           ecosystem assessments of fish assemblages in the Southern California Current and has provided  
59           decades of data on ichthyoplankton assemblages (1). The current CalCOFI surveys sample four  
60           times per year from the U.S. Mexican Border to Monterey Bay (1). We used this rich sample  
61           archive to interrogate ichthyoplankton assemblages from 1996-2019 (See Supplemental  
62           Methods). Importantly, the occurrence of a marine heatwave (MHW) within the study region and  
63           sampling period provided an additional opportunity to investigate the utility of having a non-  
64           destructive means of interrogating the valuable CalCOFI sample archive.

65

## 66       **Methods**

67       *Study Design*

68 To evaluate the efficacy of metabarcoding methods used to analyze ethanol preserved  
69 samples and investigate potential changes in the ichthyoplankton assemblages over decadal  
70 scales, we identified ichthyoplankton by metabarcoding and microscopy in ethanol-preserved  
71 samples collected over two decades (1996, 1998–2019; Figure S5) of spring CalCOFI cruises (2–  
72 5). We note that samples collected in 1997 were stored in <50% ethanol and were discarded due  
73 to failed preservation.

74 Samples were collected in late March or early April of each year  
75 (calcofi\_metadata\_analysis\_20210907.csv). Here we focus on spring samples because the  
76 majority of species in the California Current spawn in spring and historically the annual  
77 California Current Ecosystem Report has relied on the spring data (6, 7). This decision is  
78 supported by recent work using ichthyoplankton data across the full set of yearly CalCOFI  
79 cruises which found little evidence for phenological trends (6, 7), thus aiding the ability to look  
80 at impacts from the marine heatwave.

81 Samples were collected from four well-separated stations (up to 370 km apart) from  
82 distinct vicinities of the California Current with differing water properties (8) (2–5) (Figure S1).  
83 The northernmost station was located offshore of Point Conception, CA within the California  
84 Current (34.14833°N -121.1567°W). The second station was located off San Nicholas Island, CA  
85 (33.32333 °N, -119.6667 °W) that experiences high variation in annual temperature depending on  
86 the respective strengths of the California Current and Southern California Counter Current (8).  
87 The third station was a southern coastal inshore station off San Diego, CA (32.84667°N, -  
88 117.5383°W) characterized by relatively warmer waters from the California Counter Current  
89 with seasonal (spring) upwelling of cool, nutrient-rich water (8). The fourth station was a

90 southern offshore station (31.85000°N, -119.5683°W) characterized by sub-tropical oceanic  
91 waters (Figure 4).

92 At each station, oblique bongo net tows were conducted from 210 m to the surface using  
93 standard CalCOFI methods (9–12). Each side of the bongo net had a 0.71 m-diameter mouth  
94 opening and a net size of 0.505 mm mesh. Cod end contents of both bongo nets were preserved  
95 at sea. The starboard side was preserved in sodium borate-buffered 2% formaldehyde and the  
96 port side was preserved in Tris-buffered 95% ethanol. Ethanol was replaced after 24 hours to  
97 account for dilution from tissue water loss. Microscopy was conducted to identify species  
98 abundance from formaldehyde-preserved samples following standardized CalCOFI techniques  
99 (8) while metabarcoding was conducted on the ethanol in which port side samples were stored;  
100 consequently, we expected the contents of the paired samples to differ slightly as a function of  
101 sampling stochasticity.

102 *Metabarcoding Collection Isolation, Amplification, and Sequencing*

103 Prior to filtration, the ethanol-preserved samples were inverted three times and let rest for  
104 30 minutes to resuspend and homogenize samples in the preservative. Filtration of ethanol from  
105 the port-side bongo samples was conducted in a pre-PCR clean room at the NOAA Southwest  
106 Fisheries Science Center within a biological safety cabinet in July 2019. The pre-PCR room had  
107 no previous post-PCR work conducted within and all surfaces and equipment were sterilized  
108 frequently with 10% bleach and 70% ethanol. The pre-PCR clean room was at ambient pressure  
109 and reasonable precautions to limit contamination were conducted including only wearing clean  
110 clothes that have not been exposed to labs with PCR product, no food brought into the lab, and  
111 gloves were exchanged regularly.

112           Ethanol preservative was filtered using a vacuum filtration manifold with Nalgene  
113          Analytical Test Filter Funnels (Thermofisher Scientific, Waltham, MA, USA) with the  
114          manufacturer's 0.45 µm filters replaced with 0.2 µm Durapore PVDF filters (Sigma Aldrich, St.  
115          Louis, MO, USA) using sterile forceps. Up to 125 mL of ethanol was then transferred from the  
116          preserved jars into the filter funnels using a 10 mL pipette, carefully avoiding any sample  
117          contents and thus preserving CalCOFI specimens for future research and analysis. Sample jars  
118          were refilled using freshly prepared tris-buffered ethanol before being returned to the collection  
119          archive. We included two negative controls to test for lab contamination by filtering 125 mL of  
120          molecular grade water. Filters were stored at -20°C before DNA extraction.

121           Filters were extracted using the standard Qiagen DNAeasy Kit (Qiagen Inc., Valencia,  
122          CA, USA) in a pre-PCR molecular lab. Extracted DNA was amplified using the MiFish  
123          Universal Teleost primer sets to capture fish diversity (13).

124           Here, we highlight our decision to utilize the MiFish Universal Teleost *12S* primers. First,  
125          these primers have been rigorously validated for fish barcoding (14–20) and shown to provide  
126          accurate taxonomic assignments for a broad range of fishes (15). We recognize that there are  
127          limitations for this, and indeed all, metabarcoding primer sets (21) which are forced to balance  
128          specificity [how well target species can be taxonomically resolved] against breadth [range of  
129          species across the tree of life that can be amplified] (22). Even a “gold standard” like the *16S*  
130          rRNA gene marker for prokaryotic sequences struggles with taxonomic assignment accuracy  
131          (23), especially with short-read sequences. Although taxonomic resolution limitations and  
132          compromises remain for the *12S* target (15, 24), the taxonomic resolution has been improved  
133          and best practices for taxonomic classification have been identified through the development of

134 a nearly comprehensive California Current Large Marine Ecosystem *12S* reference database  
135 along with a full factorial cross-validation analysis of bioinformatic approaches (15).

136 Second, there are no widely used or benchmarked *COI* metabarcoding primer sets for  
137 fish applications although *COI* barcoding is a common barcoding target. This is because a) the  
138 conserved nature of the locus across the tree of life which results in amplification of a broad  
139 array of taxa (25, 26), and b) the mismatch in high throughput sequencing platform length  
140 (max is paired-end 300 bp) and rate of *COI* evolution/accumulation of sequence differences  
141 between species (19, 27). In fact, these shortcomings were the original motivation for  
142 researchers to develop alternative fish metabarcoding loci targeting *12S* loci for fishes (20).  
143 Together, the research community has largely converged on the MiFish Universal Teleost *12S*  
144 primer set as standard practice for fish metabarcoding given its balance of high specificity and  
145 breadth (20). Thus we feel confident that the MiFish Universal Teleost *12S* primer set was an  
146 appropriate choice for metabarcoding here.

147 Each metabarcoding extraction was subsampled for three PCR reactions using the MiFish  
148 *12S* primer set. PCR amplification for the MiFish primer set was conducted following the  
149 thermocycler profile of Curd *et al.* (16). MiFish PCR reactions had 25 µL reaction volume  
150 containing 12.5 µL QIAGEN Multiplex Taq PCR 2x Master Mix (Qiagen Inc., Valencia, CA,  
151 USA), 6.5 µL of molecular grade water, 2.5 µL of each primer (2 µmol/L), and 1 µL DNA  
152 extraction. MiFish PCR thermocycling employed a touchdown profile with an initial  
153 denaturation at 95°C for 15 min to activate the DNA polymerase, followed by 13 cycles of a 30s  
154 denaturation at 94°C, a 30s annealing that started at 69.5°C and then decreased by 1.5°C for each  
155 subsequent cycle (last cycle was 50°C), finishing with a 1 min extension at 72°C. This initial

156 touchdown profile was followed by 35 additional cycles using identical parameters except a  
157 constant annealing temperature of 50°C and ending with a final extension at 72°C for 10 min.

158 Two non-native non-marine vertebrates, American alligator (*Alligator mississippiensis*)  
159 and dromedary camel (*Camelus dromedarius*), were purchased at a local market and used as  
160 positive controls. For all positive controls, tissues were extracted using the Qiagen Blood and  
161 Tissue kit following the manufacturer's instructions. All PCR products were visualized via  
162 electrophoresis on 2% agarose gels to ensure amplification success and correct product size.  
163 Only filters from four jars failed to amplify, and upon further inspection within the archived  
164 notes, all these samples had known preservation issues (e.g., preservative dried out, observed  
165 mold, etc.). All other DNA extractions successfully amplified.

166 We prepared libraries following the methods of Curd *et al.* using a two-step PCR  
167 amplification method with one final pool per primer set. Previous work indicated that two-step  
168 PCR amplification can reduce amplification biases (28, 29) perhaps introduced by the inclusion  
169 of various indices during one-step PCR procedures. Variations in the relative amplification  
170 efficiency of each PCR is a concern here given the desire to study an array of targets in an  
171 oceanic region over space and time. Overall, there are review papers available that outline the  
172 advantages and disadvantages for one-step and two-step PCR protocols (30).

173 Prior to the second indexing PCR reaction, PCR samples from the first reaction were  
174 cleaned using the Serapure magnetic bead protocol. We quantified bead-cleaned samples with  
175 the Quant-iT™ broad range dsDNA Assay Kit (Thermofisher Scientific, Waltham, MA, USA)  
176 on a Victor3 plate reader (Perkin Elmer Waltham, MA, USA). We indexed the sample libraries  
177 using unique combinations of the Nextera Index A, B, C, and D Kit (Illumina, San Diego, CA,  
178 USA) and KAPA HiFi HotStart Ready Mix (Kapa Biosystems, Sigma Aldrich, St. Louis, MO,

179 USA). Indexing was performed with a second PCR using a 25 µL reaction mixture containing  
180 12.5 µL of Kapa HiFi Hotstart Ready mix, 1.25 µL of index primers, 10 ng of template DNA to  
181 ensure equal copy number, and the remaining volume was filled using molecular grade water  
182 depending on cleaned PCR product concentration. Index thermocycling parameters were:  
183 denaturation at 95°C for 5 min, 5 cycles of denaturation at 98°C for 20 sec, annealing at 56°C for  
184 30 sec, extension at 72°C for 3 min, followed by a final extension at 72°C for 5 min. To confirm  
185 successful PCR and correct product size, we electrophoresed PCR products on 2% agarose gels.  
186 We then bead cleaned and quantified DNA concentration, as described above so that we could  
187 pool samples so as to have equal copy number for each unique library. Pooled libraries were  
188 sequenced on an Illumina NextSeq PE 2x150 at UCLA Technology Center for Genomics and  
189 Bioinformatics.

190 *Bioinformatics*

191 The resulting metabarcoding data were processed using the *Anacapa Toolkit* to conduct  
192 quality control, amplicon sequence variant (ASV) parsing, and taxonomic assignment using user-  
193 generated custom reference databases. We processed sequences using default parameters except  
194 using a Q score cutoff of 30 and assigned taxonomy using *CRUX*-generated metabarcode  
195 specific reference databases (15). The MiFish sequencing data was assigned taxonomy using the  
196 California fish specific reference database and a bootstrap confidence cutoff score of 60  
197 following Gold *et al.* (15).

198 The two resulting raw ASV community tables were decontaminated following Kelly *et al.*  
199 (31). First, only merged paired reads that occurred at least twice (e.g., no singletons) were  
200 retained. Second, we estimated index hopping between samples by calculating the proportion of  
201 sequences within the positive control samples and then subtracting reads from each sample by

202 the sample read depth multiplied by the proportion of reads observed in the positive controls.  
203 Third, we discarded technical replicates with fewer than 30,000 reads. Fourth, we calculated  
204 Bray-Curtis dissimilarities between technical PCR replicates and fit a skewed beta distribution  
205 ( $a= 0.6$ ,  $b= 9.5$ ). We then removed all replicates with greater than 95% probability of belonging  
206 to the beta distribution. Resulting tables were then combined into a final ASV community table  
207 in *R*.

208 *Microscopy Identification of Ichthyoplankton*

209 Plankton samples were processed at the NOAA Southwest Fisheries Science Center  
210 ichthyoplankton laboratory. From each plankton sample, fish larvae were sorted and identified  
211 through microscopy to the lowest practical taxon (10, 12). Most taxa were identified to species  
212 although some were only characterized to genus or family level (See  
213 `larval_counts_20210305.csv`). The number of larvae per species per jar, total abundance of  
214 filtered ichthyoplankton, and proportion of jar sorted were recorded.

215 *Estimating Abundance*

216 We estimated the abundance of ichthyoplankton in each jar using a novel joint Bayesian  
217 hierarchical model described in detail in Supplement 2.

218 *Environmental Covariates*

219 We specifically examined the relationship of ichthyoplankton communities to sea surface  
220 temperatures (SST). Two month prior mean SSTs were obtained using the *rerddapXtracto*  
221 package (32) in *R* to collect PathFinder Ver 5.3 monthly remotely sensed composites. To  
222 calculate two-month prior means we first obtained monthly composites from April 1995 to April  
223 2019 for each station. We then averaged across monthly composite sea surface temperatures

224 ignoring any missing values. Prior two month sea surface temperatures were chosen given the  
225 average age of spring larvae (33) (Figure 4).

226 We then investigated the relationship of ichthyoplankton assemblages against sea surface  
227 temperature as a proxy for a multitude of environmental shifts associated with the MHW. In  
228 addition, we specifically characterized fish that are uniquely present or absent before (1996-  
229 2013) and after the 2014-16 Marine Heatwave (2014-2019). Analyses were repeated using the  
230 mean average water column temperature (MWCT) obtained from nearly simultaneously  
231 conducted CTD rosette deployments (9). The mean water column temperature was averaged  
232 across 10 to 100m depth, where the majority of ichthyoplankton reside, following Thompson et  
233 al. (9).

234 *Data Analysis*

235 After model estimation, we calculated mean abundance estimates (larvae counts per  
236 standardized volume towed) per species per station per year. To explore species-specific sea  
237 surface temperature (SST) relationships, we fit a Bayesian generalized linear model using log  
238 (abundance) as the response variable and SST ( $^{\circ}\text{C}$ ) as a continuous predictor variable. Models  
239 were implemented for each species using Stan as implemented in R (34). We then summarized  
240 the affinity between each species and SST by calculating a T-statistic based on each species'  
241 estimated coefficients (mean slope/standard deviation). We further plotted the estimated slope  
242 for each “species grouping” by habitat associations derived from previous CalCOFI research  
243 (habitat\_association\_to\_check\_art.csv)(35). We summed total log(abundance) per habitat  
244 association per station per year and fit a Bayesian generalized linear model using log (total  
245 abundance) as the response variable and SST ( $^{\circ}\text{C}$ ) as a continuous predictor variable.

246 We repeated the above analyses using a Bayesian binomial model using presence as the  
247 response variable and SST ( $^{\circ}\text{C}$ ) as a continuous predictor variable across the data set to explore  
248 occurrence relationships with temperature and identify warm- and cool- associated taxa. We set a  
249 threshold of presence/absence based on the model using a threshold of  $< 0.01$  larvae per  
250 standardized volume to be considered absent within a station.

251 We further explored species occurrence and abundance relationships with SST by fitting  
252 the above Bayesian generalized linear models with station as a random effect. In addition, we  
253 repeated all of the above analyses using MWCT instead of SST.

254 To explore how fish assemblages change over time we plotted a heatmap of observed  
255 abundance summed across stations each year. Chronological clustering was conducted across  
256 years using Bray Curtis dissimilarities of abundances using a K of 8 using the package *rioja* in R  
257 (36) and a dendrogram of years was constructed using the *ggdenro* package (37). Similarly,  
258 hierarchical clustering was conducted across species using Bray Curtis dissimilarities of  
259 abundances using a K of 6. To further explore fish assemblage changes NMDS Ordination of  
260 Bray-Curtis dissimilarities were calculated from estimated abundances of each year summed  
261 across stations as implemented by the *metaMDS* function from *vegan* in R (38). The above  
262 analyses were also conducted with station separated as well as each station on it's own. To  
263 investigate the relative effect of year, SST, and station to the explained variance in fish  
264 assemblages across the ata set, we ran a PERMANOVA on Bray-Curtis dissimilarities using the  
265 following model: ~ Year + SST + station.

266 We visualized anchovy and sardine abundance over time by calculating the median log  
267 (abundance) of each species per station per year. We then plotted the log (median) abundance of

268 each of the four stations while error bars represent the 95% confidence intervals observed for a  
269 given species at a given station in that year.

270 To explore co-occurrence patterns across species, we fit a generalized linear latent  
271 variable model (GLLVM) following the methods of Niku et al. (39), specifically conducting  
272 model fitting to determine the best distribution fit as well as number of latent variables to use.

273 The highest performing GLLVM employed 3 latent variables and applied a negative binomial  
274 distribution with variational approximation (40) on the joint model predicted larvae count data.

275 We then plotted the correlation matrix of the linear predictors across species with and without  
276 incorporating SST in the GLLVM to identify co-occurring species and the effect of SST on co-  
277 occurrence patterns.

278 To evaluate the effect of the marine heatwave (MHW) on CCLME fishes we compared  
279 estimated species abundances before the MHW (1996-2013), to both during and after the MHW  
280 (2014-2019), at each station respectively. We first calculated the mean abundance for each  
281 species at each station for each model run. We then subtracted the means for each model run to  
282 evaluate changes in MHW abundance per species per station per model run. We then calculated a  
283 95% CI of change in MHW abundance per species to identify which species were significantly  
284 different before vs. during and after the MHW at each station.

285 All data and code to conduct analyses and generate all figures are available on GitHub  
286 ([https://github.com/zjgold/CalCOFI\\_eDNA](https://github.com/zjgold/CalCOFI_eDNA)) and associated Google Drive link  
287 ([https://drive.google.com/drive/folders/12cU9mY\\_CWoro-x6Hgh\\_pgv\\_66zZEzm1h?usp=sharing](https://drive.google.com/drive/folders/12cU9mY_CWoro-x6Hgh_pgv_66zZEzm1h?usp=sharing)) [will be replaced with a Dryad repository upon  
289 acceptance].

290

291 **Results**

292 *Fish Assemblage Structure*

293 We observed substantial changes in fish assemblage structure across stations, time, and  
294 temperature sampled (NMDS stress =0.03) (Figure S11-26). station explained the greatest  
295 observed variance (12%) which is unsurprising given the intentionally chosen distinct  
296 biogeographic characteristics of each station (PERMANOVA p <0.05). However, despite the >  
297 370km distance between stations, we captured significant synchronous changes in fish  
298 assemblage dynamics in response to year (2.4%) and temperature (4.6%) (PERMANOVA p  
299 <0.05). In particular, we observed strong clustering of the post MHW period from 2017-2019,  
300 the 2005 El Niño and the 1998 El Niño along with southern mesopelagic species. Both 2014 and  
301 2016 were distinct from other years and associated with a suite of mesopelagic species, although  
302 the MHW itself was not strongly clustered largely due to the differential onset and  
303 characterization of the warming event within the region (3).

304 We also found strong positive and negative co-occurrence patterns through GLLVM  
305 analyses across species when controlling for temperature. Specifically, we observed strong  
306 negative co-occurrence patterns between fisheries targets like benthic fisheries targets (e.g.  
307 *Citharichthys* sp. sanddabs) and mesopelagic fishes (S27). We also observed strong positive co-  
308 occurrence patterns between a suite of benthic species as well as strong positive co-occurrence  
309 patterns between a suite of mesopelagic fishes. These results suggest that when controlling for  
310 temperature, we observe strong benthic versus pelagic tradeoffs as observed previously (6, 41,  
311 42).

312 When focusing on co-occurrence patterns without controlling for temperature, we  
313 observed strong negative co-occurrence patterns with fisheries targets (North Pacific Hake

314 *Merluccius productus*) and mesopelagic fishes (S28). Here, temperature explained 19% of the  
315 variability among species co-occurrence and was particularly important in driving negative co-  
316 occurrence patterns between North Pacific Hake and mesopelagic species. These results suggest  
317 that temperature may mediate tradeoffs between fisheries versus southern mesopelagic fish  
318 assemblages. Further work exploring the underlying mechanisms of these negative co-  
319 occurrence patterns is warranted.

320 *Analysis Using Mean Water Column Temperature*

321 We repeated the analyses presented in the main manuscript with mean water column  
322 temperature (MWCT) as opposed to two-month SST (Figures 1-3). Two-month averaged SST  
323 and instantaneous MWCT were only 29% correlated (linear regression,  $p < 0.01$ ). This finding is  
324 perhaps unsurprising given the substantial difference in spatial and temporal integration time of  
325 these temperature measurements. Despite these apparent differences, we found nearly identical  
326 results in the direction and significance of species–temperature associations as well as  
327 temperature-driven variation in fish assemblage dynamics (Figures S6–S13). These results  
328 suggest that species–temperature associations and our conclusions are largely robust to  
329 temperature metrics.

330 *Metabarcoding Signal Appears Stable in the Ethanol-Preserved Samples*

331 For each station-species combination, if metabarcoding signals appear auto-correlated in  
332 time -- that is, if one year's metabarcoding signal is correlated with the previous year's signal --  
333 then we require a time-series model that incorporates such autocorrelation into the error  
334 structure. If, by contrast, years appear independent of one another, we can treat model variation  
335 as time-independent and therefore treat each data point as being independent. We observe no

336 such correlation (mean = -0.014, standard deviation = 0.35) and so we treat all observations as  
337 independent of one another.

338 In further investigating the question of whether these samples can be considered time-  
339 independent, we considered whether or not older samples might have less metabarcoding signal  
340 due to sample degradation. If the metabarcoding signal were degrading overtime in the preserved  
341 samples, we would expect several parameters to change as a function of sample age: (1) a  
342 decrease in precision with which we observe amplicon abundance, (2) a decrease in richness of  
343 species detected, and (3) a decrease in the confidence in posterior estimates of larval abundances  
344 from our joint Bayesian model. We test for these effects in turn.

345 First, among triplicate PCR reactions, we might expect degraded DNA to behave more  
346 stochastically than non-degraded DNA, such that technical replicates would yield increasingly  
347 divergent amplicon abundances with greater degradation. Here, we measure the precision of our  
348 estimates with the coefficient of variation (CV) of species-specific amplicons across three  
349 technical replicates. An increase in CV with the age of the sample would signal degradation, but  
350 we saw no such trend (Figure S29). Second, rare amplicons often make up a large fraction of  
351 metabarcoding datasets, and because of their rarity, these often show up stochastically across  
352 replicates or sequenced samples. If older DNA samples were degraded, we would expect fewer  
353 of these rare species, and by extension, fewer species overall. We saw no such effect (linear  
354 regression  $p > 0.5$ ; linear mixed effect model failed convergence). Third, we might expect -- if  
355 DNA were degrading -- that such degradation would impair our ability to estimate the larval  
356 abundance of each species in older samples. Again, we saw no evidence of this effect (Figure  
357 S30-31).

358 *Overlap in Species Detections*

359 The maximum observed morphological counts in which metabarcoding failed to detect a given  
360 taxa was 9 (mean = 1.61). Across a total of 4,704 possible detections, 70.2% were non-detections  
361 by both methods, 11.2% were detections by both methods, 16.4% were detections only made by  
362 metabarcoding, and 2.1% were detections only made my microscopy (Figure S4).

363 *Stochasticity in Metabarcoding Data*

364 We conducted a deep dive into the origin and source of variation in amplicon sequence data.  
365 These analyses identified stochastic dropouts in whereby a taxon is amplified in one PCR  
366 reaction but not in a replicate PCR reaction as a main driver of variation in this data set. This is a  
367 well-known phenomenon general to PCR with rare templates (43–45) and we document such  
368 behavior in this manuscript (Figures S2-S4). For example, for *Symbolophorus californiensis* we  
369 observed an instance of 3,897 reads, 165 reads, and 0 reads across three technical PCR replicates  
370 with sample read depths of 132,731, 196,260, 55,400 from the same DNA extraction. These  
371 stochastic dropouts are easily visualized along the X axis in Figure S2. We note that the highest  
372 observed species-specific amplicon sample read proportion associated with a stochastic dropout  
373 was 2.9% (3,897 /132,731) with the vast majority of such dropouts occurring below 0.03% read  
374 proportion within a technical replicate. These results suggest that stochasticity is largely driven  
375 by the abundance of DNA molecules within a sample rather than a specific feature associated  
376 with a particular primer set, especially given that dozens of other metabarcoding studies have  
377 identified similar patterns (44–46).

378 This phenomenon of stochastic dropouts adds noise to the observations and limits the  
379 accuracy with which we might predict amplicon abundances (particularly rare ones). This is  
380 best visualized by the noise near the origin at Figures S3 & S4. To address this, we developed a  
381 comprehensive joint Bayesian model that incorporates stochasticity in observed amplicon read

382 counts through a multinomial subsampling process (See supplement 2 for full model  
383 description). Thus, we explicitly account for stochasticity in the model through sampling  
384 distributions and using the resulting parameters to estimate the uncertainty around our given  
385 estimated larvae counts. Ultimately, such noise in the dataset does not fundamentally change  
386 the interpretation of our observations or of our model but serves to limit our confidence in the  
387 abundance of rare targets, a persistent problem in community ecology (47).

388

389

## 390 **References**

- 391 1. J. N. Heine, California Cooperative Oceanic Fisheries Investigations. Reports. **49**, 264  
392 (2008).
- 393 2. A. R. Thompson, C. J. Harvey, W. J. Sydeman, C. Barceló, S. J. Bograd, R. D. Brodeur, J.  
394 Fiechter, J. C. Field, N. Garfield, T. P. Good, E. L. Hazen, M. E. Hunsicker, K. Jacobson,  
395 M. G. Jacox, A. Leising, J. Lindsay, S. R. Melin, J. A. Santora, I. D. Schroeder, J. A.  
396 Thayer, B. K. Wells, G. D. Williams, Indicators of pelagic forage community shifts in the  
397 California Current Large Marine Ecosystem, 1998–2016. *Ecol. Indic.* **105**, 215–228  
398 (2019).
- 399 3. J. M. Nielsen, L. A. Rogers, R. D. Brodeur, A. R. Thompson, T. D. Auth, A. L. Deary, J.  
400 T. Duffy-Anderson, M. Galbraith, J. A. Koslow, R. I. Perry, Responses of ichthyoplankton  
401 assemblages to the recent marine heatwave and previous climate fluctuations in several  
402 Northeast Pacific marine ecosystems. *Glob. Chang. Biol.* **27**, 506–520 (2021).
- 403 4. A. S. Ren, D. L. Rudnick, Temperature and salinity extremes from 2014-2019 in the  
404 California Current System and its source waters. *Commun. Earth Environ.* **2**, 1–9 (2021).

- 405 5. E. D. Weber, T. D. Auth, S. Baumann-Pickering, T. R. Baumgartner, E. P. Bjorkstedt, S.  
406 J. Bograd, B. J. Burke, J. L. Cadena-Ramírez, E. A. Daly, M. de la Cruz, State of the  
407 California Current 2019–2020: Back to the Future With Marine Heatwaves? *Front. Mar.*  
408 *Sci.*, 1081 (2021).
- 409 6. A. R. Thompson, N. J. Ben-Aderet, N. M. Bowlin, D. Kacev, R. Swalethorp, W. Watson,  
410 Putting the Pacific marine heatwave into perspective: The response of larval fish off  
411 southern California to unprecedented warming in 2014–2016 relative to the previous 65  
412 years. *Glob. Chang. Biol.* **28**, 1766–1785 (2022).
- 413 7. S. McClatchie, J. Gao, E. J. Drenkard, A. R. Thompson, W. Watson, L. Ciannelli, S. J.  
414 Bograd, J. T. Thorson, Interannual and Secular Variability of Larvae of Mesopelagic and  
415 Forage Fishes in the Southern California Current System. *J. Geophys. Res. Ocean.* **123**,  
416 6277–6295 (2018).
- 417 8. S. McClatchie, A. R. Thompson, S. R. Alin, S. Siedlecki, W. Watson, S. J. Bograd, The  
418 influence of Pacific Equatorial Water on fish diversity in the southern California Current  
419 System. *J. Geophys. Res. Ocean.* **121**, 6121–6136 (2016).
- 420 9. A. R. Thompson, W. Watson, S. McClatchie, E. D. Weber, Multi-scale sampling to  
421 evaluate assemblage dynamics in an oceanic marine reserve. *PLoS One.* **7**, e33131 (2012).
- 422 10. A. R. Thompson, S. McClatchie, E. D. Weber, W. Watson, C. E. Lennert-Cody,  
423 Correcting for bias in calcofi ichthyoplankton abundance estimates associated with the  
424 1977 transition from ring to bongo net sampling. *Calif. Coop. Ocean. Fish. Investig.*  
425 *Reports.* **58**, 1–11 (2017).
- 426 11. D. Kramer, M. J. Kalin, E. G. Stevens, J. R. Thraikill, J. Zweifel, *Collecting and*  
427 *processing data on fish eggs and larvae in the California Current. NOAA Tech. Rep.*

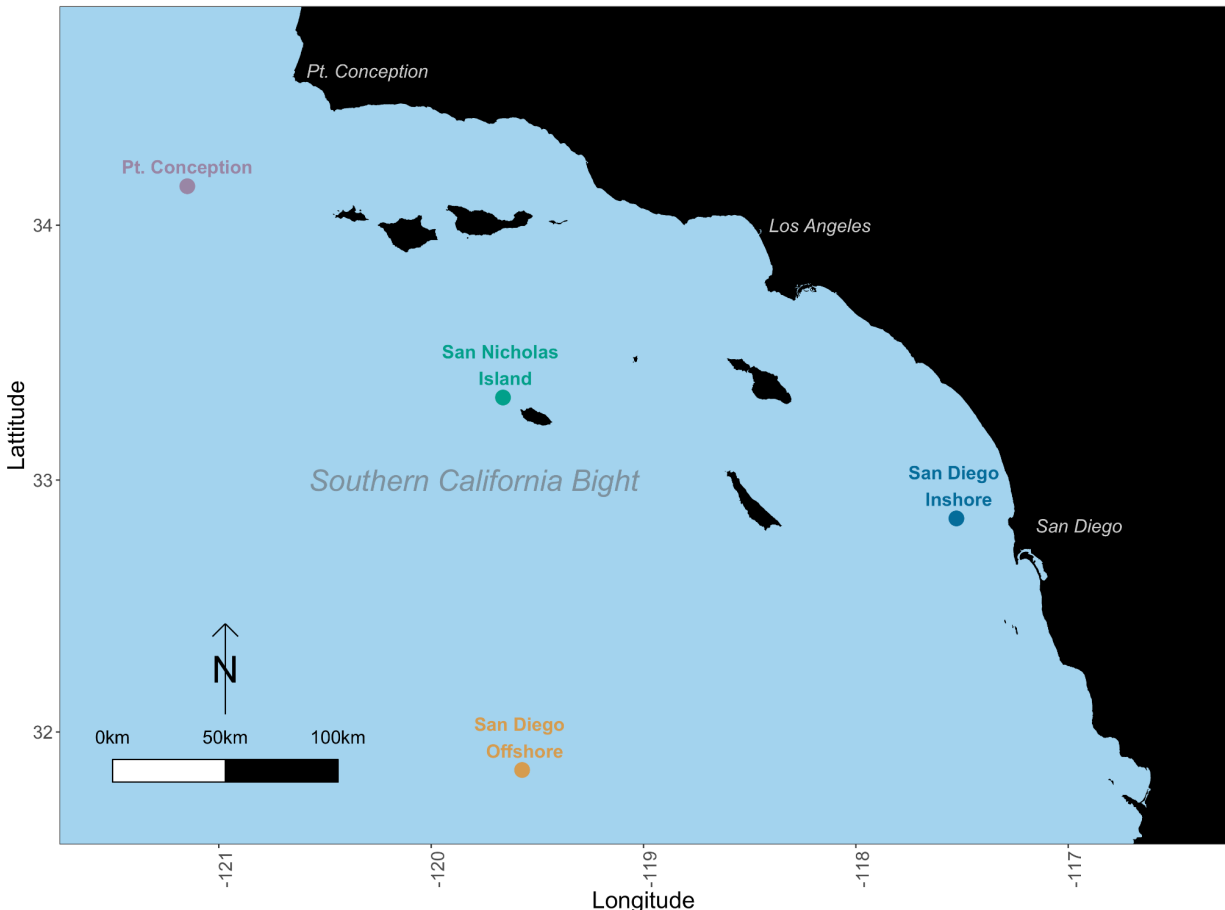
- 428        *NMFS Circ.*, vol. 370. (US Department of Commerce, National Oceanic and Atmospheric  
429        Administration ..., 1972), vol. 370.
- 430        12. S. McClatchie, *Regional fisheries oceanography of the California current system: The  
431        CalCOFI program* (Springer, 2014).
- 432        13. M. Miya, Y. Sato, T. Fukunaga, T. Sado, J. Y. Poulsen, K. Sato, T. Minamoto, S.  
433        Yamamoto, H. Yamanaka, H. Araki, M. Kondoh, W. Iwasaki, MiFish, a set of universal  
434        PCR primers for metabarcoding environmental DNA from fishes: Detection of more than  
435        230 subtropical marine species. *R. Soc. Open Sci.* **2**, 150088 (2015).
- 436        14. M. Miya, Y. Sato, T. Fukunaga, T. Sado, J. Y. Poulsen, K. Sato, T. Minamoto, S.  
437        Yamamoto, H. Yamanaka, H. Araki, M. Kondoh, W. Iwasaki, MiFish, a set of universal  
438        PCR primers for metabarcoding environmental DNA from fishes: Detection of more than  
439        230 subtropical marine species. *R. Soc. Open Sci.* **2**, 150088 (2015).
- 440        15. Z. Gold, E. E. Curd, K. D. Goodwin, E. S. Choi, B. W. Frable, A. R. Thompson, H. J.  
441        Walker, R. S. Burton, D. Kacev, L. D. Martz, P. H. Barber, Improving metabarcoding  
442        taxonomic assignment: A case study of fishes in a large marine ecosystem. *Mol. Ecol.*  
443        *Resour.* **21**, 2546–2564 (2021).
- 444        16. E. E. Curd, Z. Gold, G. S. Kandlikar, J. Gomer, M. Ogden, T. O’Connell, L. Pipes, T. M.  
445        Schweizer, L. Rabichow, M. Lin, B. Shi, P. H. Barber, N. Kraft, R. Wayne, R. S. Meyer,  
446        Anacapa Toolkit: An environmental DNA toolkit for processing multilocus metabarcode  
447        datasets. *Methods Ecol. Evol.* **10**, 1469–1475 (2019).
- 448        17. E. Valsecchi, J. Bylemans, S. J. Goodman, R. Lombardi, I. Carr, L. Castellano, A.  
449        Galimberti, P. Galli, Novel universal primers for metabarcoding environmental DNA  
450        surveys of marine mammals and other marine vertebrates. *Environ. DNA.* **2**, 460–476

- 451 (2020).
- 452 18. R. A. Collins, G. Trauzzi, K. M. Maltby, T. I. Gibson, F. C. Ratcliffe, J. Hallam, S.  
453 Rainbird, J. Maclaine, P. A. Henderson, D. W. Sims, S. Mariani, M. J. Genner, Meta-Fish-  
454 Lib: A generalised, dynamic DNA reference library pipeline for metabarcoding of fishes.  
455 *J. Fish Biol.* **99**, 1446–1454 (2021).
- 456 19. A. Polanco F., E. Richards, B. Flück, A. Valentini, F. Altermatt, S. Brosse, J. C. Walser,  
457 D. Eme, V. Marques, S. Manel, C. Albouy, T. Dejean, L. Pellissier, Comparing the  
458 performance of 12S mitochondrial primers for fish environmental DNA across  
459 ecosystems. *Environ. DNA.* **3**, 1113–1127 (2021).
- 460 20. M. Miya, R. O. Gotoh, T. Sado, MiFish metabarcoding: a high-throughput approach for  
461 simultaneous detection of multiple fish species from environmental DNA and other  
462 samples. *Fish. Sci.* **86**, 939–970 (2020).
- 463 21. K. Deiner, H. M. Bik, E. Mächler, M. Seymour, A. Lacoursière-Roussel, F. Altermatt, S.  
464 Creer, I. Bista, D. M. Lodge, N. de Vere, M. E. Pfrender, L. Bernatchez, Environmental  
465 DNA metabarcoding: Transforming how we survey animal and plant communities. *Mol.*  
466 *Ecol.* **26**, 5872–5895 (2017).
- 467 22. P. Taberlet, A. Bonin, L. Zinger, E. Coissac, *Environmental DNA: For biodiversity*  
468 *research and monitoring* (Oxford University Press, 2018).
- 469 23. R. C. Edgar, Accuracy of taxonomy prediction for 16S rRNA and fungal ITS sequences.  
470 *PeerJ.* **2018**, e4652 (2018).
- 471 24. M. A. Min, P. H. Barber, Z. Gold, MiSebastes: An eDNA metabarcoding primer set for  
472 rockfishes (genus *Sebastes*). *Conserv. Genet. Resour.* **13**, 447–456 (2021).
- 473 25. M. Leray, J. Y. Yang, C. P. Meyer, S. C. Mills, N. Agudelo, V. Ranwez, J. T. Boehm, R.

- 474 J. Machida, A new versatile primer set targeting a short fragment of the mitochondrial  
475 COI region for metabarcoding metazoan diversity: Application for characterizing coral  
476 reef fish gut contents. *Front. Zool.* **10**, 34 (2013).
- 477 26. P. A. Hastings, R. S. Burton, Establishing a DNA Sequence database for the marine fish  
478 fauna of California, 5 (2008).
- 479 27. B. E. Deagle, S. N. Jarman, E. Coissac, F. Pompanon, P. Taberlet, DNA metabarcoding  
480 and the cytochrome c oxidase subunit I marker: Not a perfect match. *Biol. Lett.* **10**,  
481 20140562 (2014).
- 482 28. J. L. O'donnell, R. P. Kelly, N. C. Lowell, J. A. Port, Indexed PCR primers induce  
483 template- Specific bias in Large-Scale DNA sequencing studies. *PLoS One.* **11**, e0148698  
484 (2016).
- 485 29. D. M. Gohl, P. Vangay, J. Garbe, A. MacLean, A. Hauge, A. Becker, T. J. Gould, J. B.  
486 Clayton, T. J. Johnson, R. Hunter, D. Knights, K. B. Beckman, Systematic improvement  
487 of amplicon marker gene methods for increased accuracy in microbiome studies. *Nat.*  
488 *Biotechnol.* **34**, 942–949 (2016).
- 489 30. K. Bohmann, V. Elbrecht, C. Carøe, I. Bista, F. Leese, M. Bunce, D. W. Yu, M. Seymour,  
490 A. J. Dumbrell, S. Creer, Strategies for sample labelling and library preparation in DNA  
491 metabarcoding studies. *Mol. Ecol. Resour.* (2021), doi:10.1111/1755-0998.13512.
- 492 31. R. P. Kelly, R. Gallego, E. Jacobs-Palme, The effect of tides on nearshore environmental  
493 DNA. *PeerJ.* **2018**, e4521 (2018).
- 494 32. R. Mendelsohn, rerdapXtracto: Extracts Environmental Data from “ERDDAP” Web  
495 Services. R package version 1.0.0 (2020).
- 496 33. H. G. Moser, R. L. Charter, W. Watson, D. A. Ambrose, K. T. Hill, P. E. Smith, J. L.

- 497        Butler, E. M. Sandknop, S. R. Charter, The CalCOFI ichthyoplankton time series:
- 498        Potential contributions to the management of rocky-shore fishes. *Calif. Coop. Ocean.*
- 499        *Fish. Investig. Reports.* **42**, 112–128 (2001).
- 500        34. B. Goodrich, J. Gabry, I. Ali, S. Brilleman, rstanarm: Bayesian applied regression
- 501        modeling via Stan. *R Packag. version.* **2**, 1758 (2020).
- 502        35. C. H. Hsieh, C. Reiss, W. Watson, M. J. Allen, J. R. Hunter, R. N. Lea, R. H. Rosenblatt,
- 503        P. E. Smith, G. Sugihara, A comparison of long-term trends and variability in populations
- 504        of larvae of exploited and unexploited fishes in the Southern California region: A
- 505        community approach. *Prog. Oceanogr.* **67**, 160–185 (2005).
- 506        36. S. Juggins, rioja: Analysis of Quaternary science data, R package version (0.9-9). *Compr.*
- 507        *r Arch. Netw.* (2015).
- 508        37. A. de Vries, B. D. Ripley, Create Dendograms and Tree Diagrams Using “ggplot2.” *URL*
- 509        <https://github.com/andrie/ggdendro>, 12 (2020).
- 510        38. J. Oksanen, F. G. Blanchet, R. Kindt, P. Legendre, P. R. Minchin, O. R.B., G. L. Simpson,
- 511        P. Solymos, M. H. H. Stevens, H. Wagner, vegan: Community ecology package. *R*
- 512        *Packag. version* 2.3-5 (2016), (available at <https://cran.r-project.org/package=vegan>).
- 513        39. J. Niku, F. K. C. Hui, S. Taskinen, D. I. Warton, gllvm: Fast analysis of multivariate
- 514        abundance data with generalized linear latent variable models in r. *Methods Ecol. Evol.*
- 515        **10**, 2173–2182 (2019).
- 516        40. A. Kucukelbir, R. Ranganath, A. Gelman, D. Blei, Automatic variational inference in
- 517        Stan. *Adv. Neural Inf. Process. Syst.* **28** (2015).
- 518        41. P. E. Smith, H. G. Moser, Long-term trends and variability in the larvae of Pacific sardine
- 519        and associated fish species of the California Current region. *Deep. Res. Part II Top. Stud.*

- 520                  *Oceanogr.* **50**, 2519–2536 (2003).
- 521    42. H. G. Moser, R. L. Charter, P. E. Smith, D. A. Ambrose, S. R. Charter, C. A. Meyer, E.  
522                  M. Sandknop, W. Watson, *Distributional atlas of fish larvae and eggs in the California*  
523                  *Current region: taxa with 1000 or more total larvae, 1951 through 1984* (Marine Life  
524                  Research Program, Scripps Institution of Oceanography, 1993), vol. 53.
- 525    43. M. Leray, N. Knowlton, Random sampling causes the low reproducibility of rare  
526                  eukaryotic OTUs in Illumina COI metabarcoding. *PeerJ.* **2017**, e3006 (2017).
- 527    44. R. Jiang, W. V. Li, J. J. Li, mbImpute: an accurate and robust imputation method for  
528                  microbiome data. *Genome Biol.* **22**, 1–27 (2021).
- 529    45. J. D. Silverman, K. Roche, S. Mukherjee, L. A. David, Naught all zeros in sequence count  
530                  data are the same. *Comput. Struct. Biotechnol. J.* **18**, 2789–2798 (2020).
- 531    46. J. J. Jos', J. Egozcue, J. Graffelman, M. I. Ortego, V. Pawlowsky-Glahn, Some thoughts  
532                  on counts in sequencing studies. *NAR Genomics Bioinforma.* **2**, 1–10 (2020).
- 533    47. J. A. Royle, W. A. Link, Generalized station occupancy models allowing for false positive  
534                  and false negative errors. *Ecology.* **87**, 835–841 (2006).
- 535
- 536



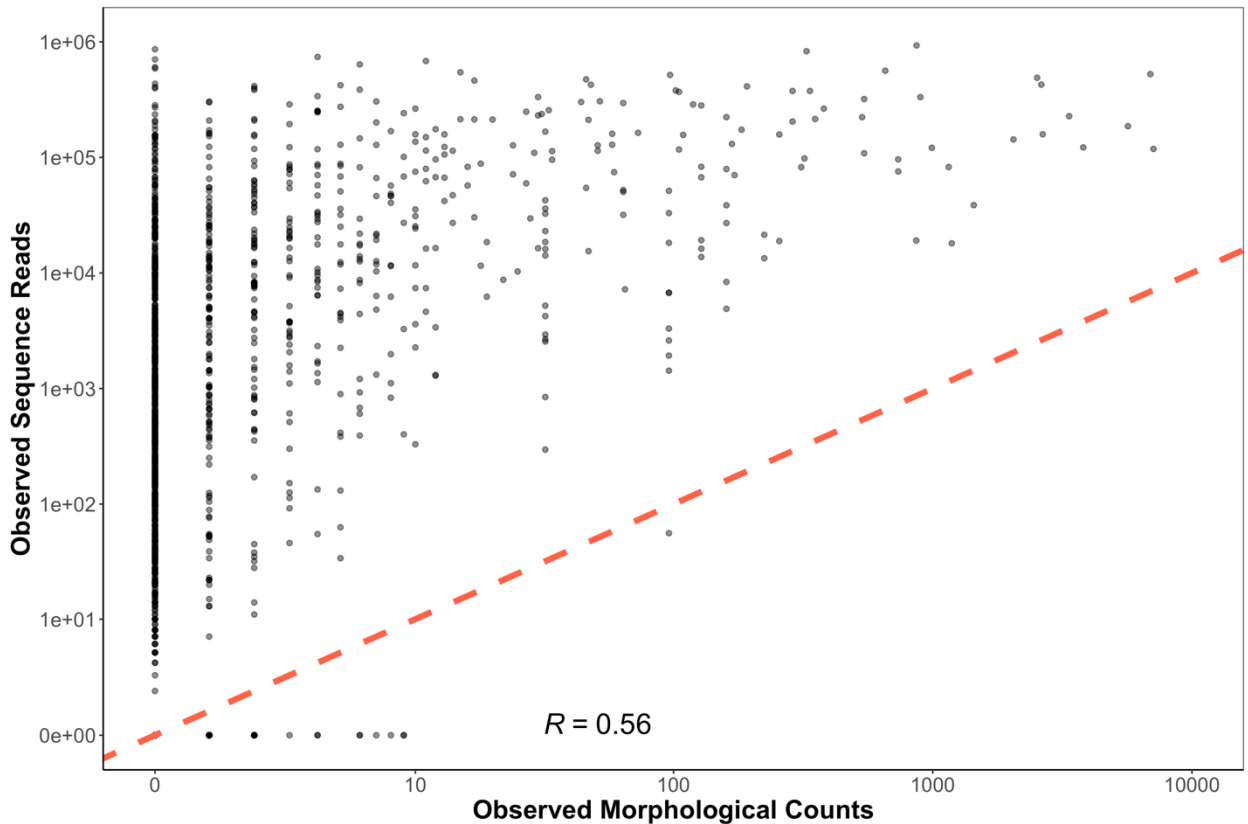
537

538 **Figure S1. station Map**

539 Ichthyoplankton samples were collected from four stations with distinct biogeographic  
540 characteristics.

541

542



543

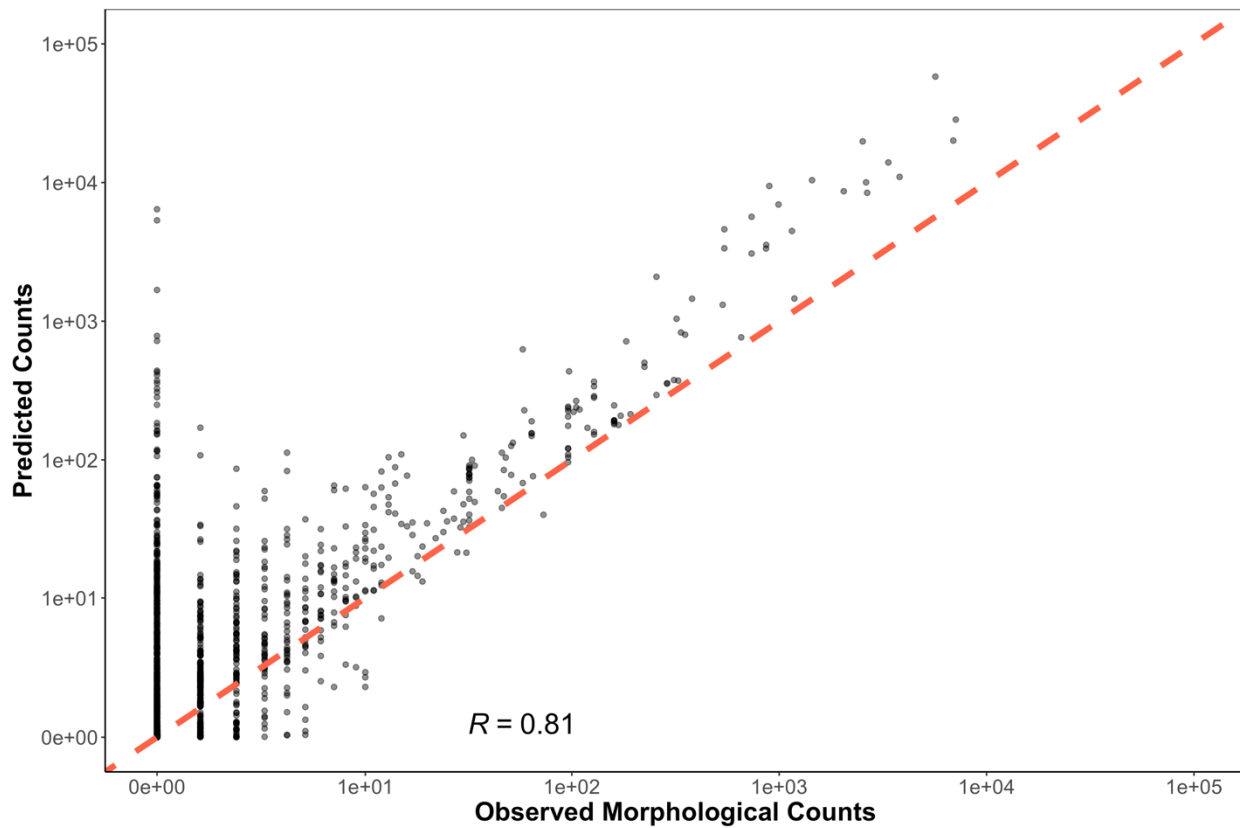
544

**545 Figure S2. Observed Sequence Reads vs. Observed Morphological Counts**

546 Observed sequencing reads and morphological counts do not follow a clear linear  
 547 relationship. The one-to-one line is plotted in red and Pearson correlation coefficient is  
 548 0.56. This non-linearity is unsurprising given that observed reads are a function of both  
 549 DNA concentrations (here assumed proportional to morphological counts) as well as  
 550 species-specific amplification efficiencies (here are unknown) (See Supplement 2). Thus  
 551 without accounting for species-specific amplification efficiencies within the compositional  
 552 amplicon data set, we do not expect to observe a clear positive relationship. This apparent  
 553 lack of relationship depicted here motivated the creation of the mechanistic joint Bayesian  
 554 model. We also note the occurrence of stochastic dropouts (technical replicates with zero  
 555 reads) can be observed along the X-axis. We also note that variance is highest at low

556 observed morphological counts.

557



558

559

560 **Figure S3. Predicted Counts vs. Observed Morphological Counts**

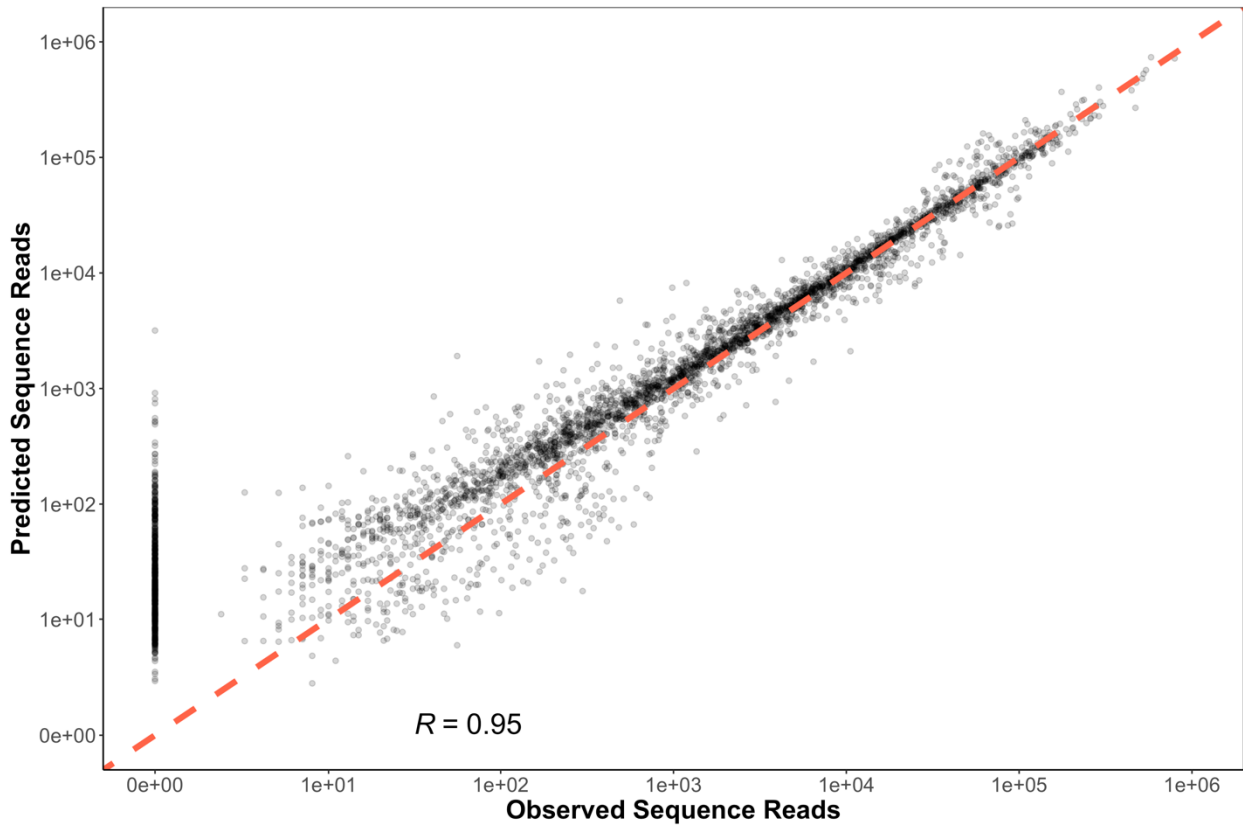
561 Predicted counts are generated from the joint Bayesian model. The one-to-one line is  
562 plotted in red and Pearson correlation coefficient is 0.81. Variance in predicted counts  
563 markedly decreases with higher observed morphological counts. We note variance in  
564 predicted counts is substantially less than that between observed reads and morphological  
565 counts Figure S3.

566

567

568

569



570

571

572

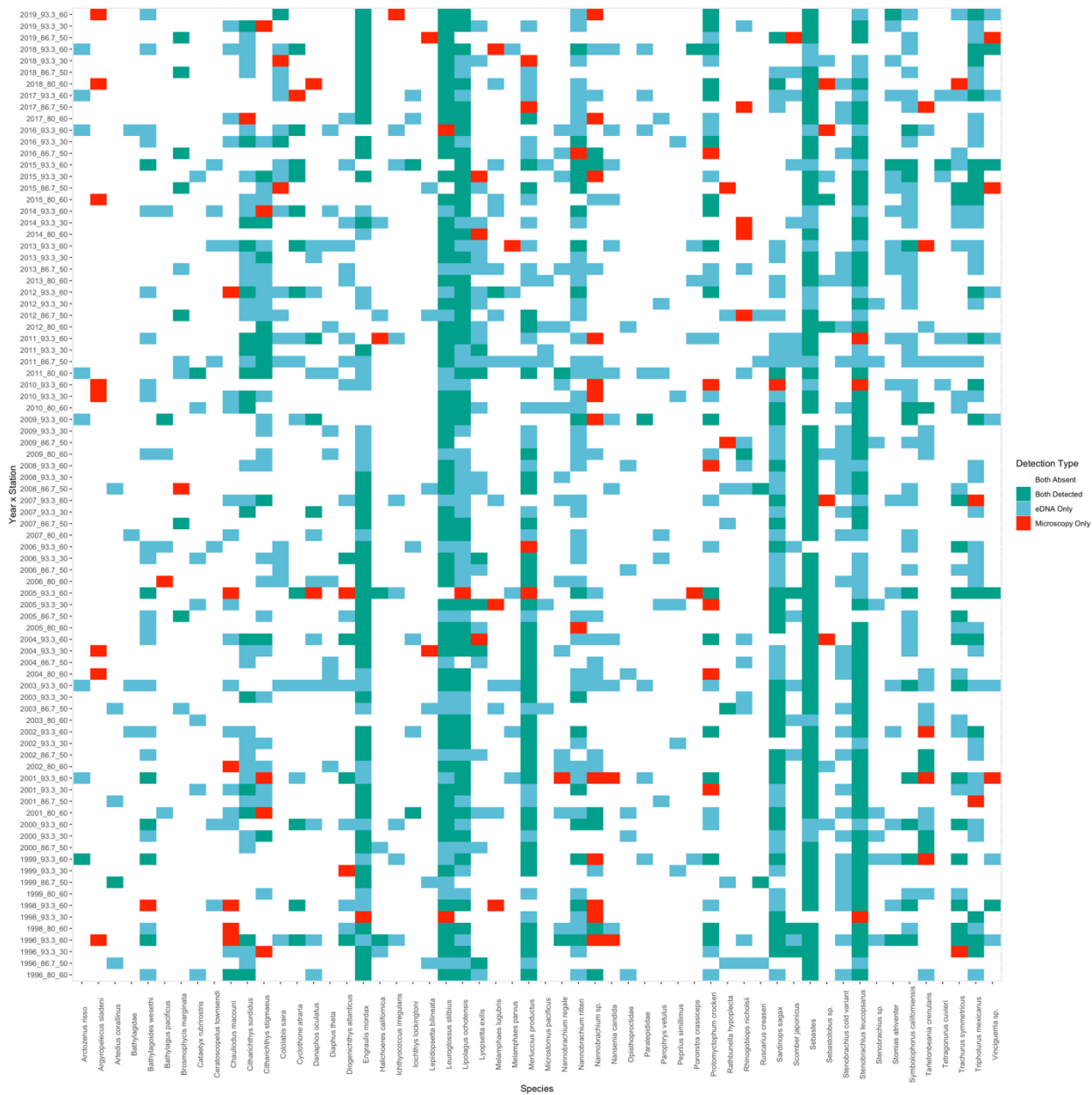
573 **Figure S4. Predicted Sequence Reads vs. Observed Sequence Reads**

574 Predicted sequence reads are generated from the joint Bayesian model. The one-to-one  
575 line is plotted in red and Pearson correlation coefficient is 0.95. In general, predicted  
576 sequence reads track observed sequence reads, and show substantially less variance than  
577 observed sequence reads in Figure S3. However, unexpected zeros across multiple  
578 technical PCR replicates (stochastic dropouts), deviate notably from expected, low  
579 variance results (points along Y-axis). We note that all observed stochastic dropouts occur  
580 in less than 2.9% of sample read proportions and less than 9 morphological counts for a  
581 given sample. Such dropouts are likely a function of subsampling rare DNA molecules

582

associated with molecular biology processing (See Supplement 2).

583



584

### Figure S5. Co-detection of Taxa By Metabarcoding and Microscopy

585

Of the 56 taxa used for modeling efforts (Supplemental Methods), both metabarcoding

586

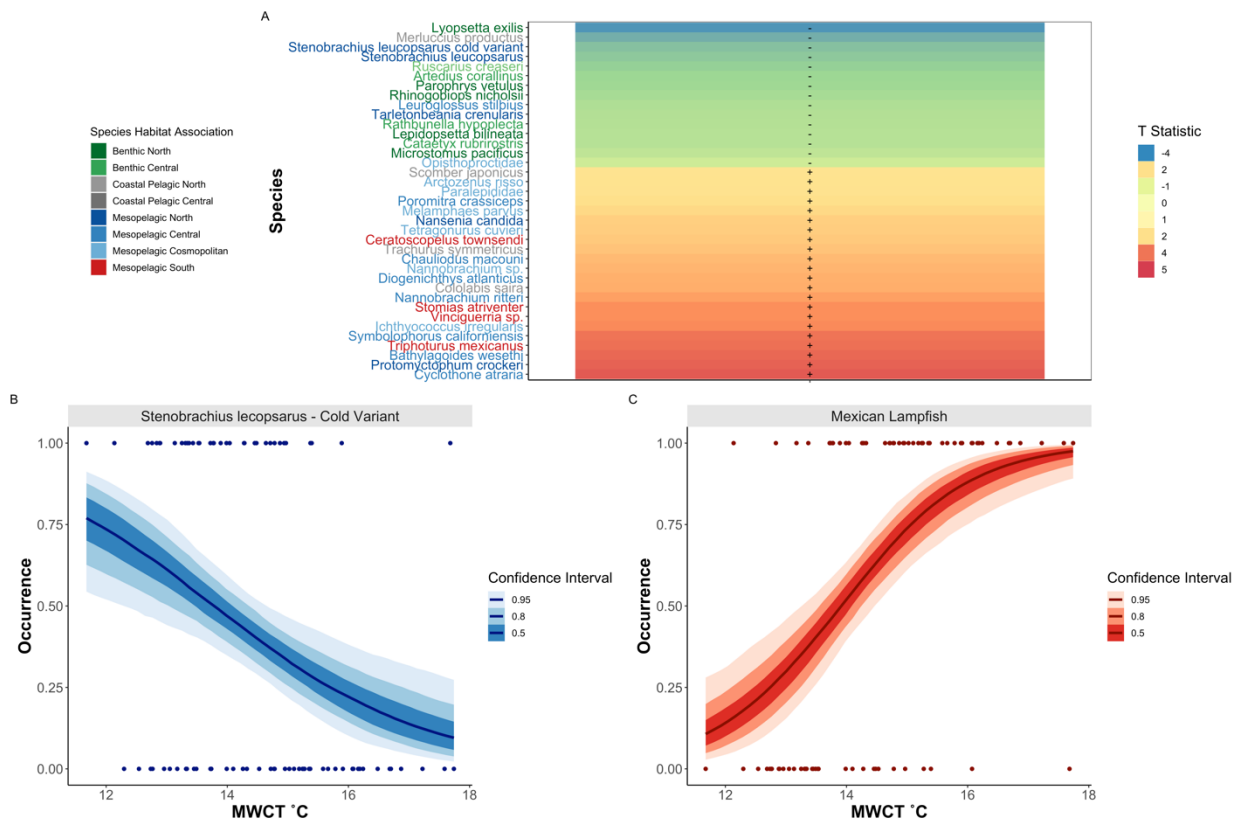
and microscopy detected 46 taxa, with nine detected only by metabarcoding and one

587

detected only by microscopy.

589

590



591

### 592 Figure S6. Temperature Associations in Fish Species

593 Changes in species occurrence patterns in response to MWCT, with Southern  
 594 Mesopelagic species increasing in prevalence with elevated temperature (A). T statistic  
 595 (slope coefficient/ standard error) from generalized binomial mixed model was calculated  
 596 for each species across all stations. Only species with significantly different slopes (95%  
 597 CI greater or less than zero) are plotted. Importantly, metabarcoding identified cold  
 598 associated variants of the Northern Lanternfish (*Stenobrachius leucopsarus*) which  
 599 cannot be morphologically identified (B) as well as warm-associated species like the  
 600 Mexican Lampfish (*Triphoturus mexicanus*) (C).

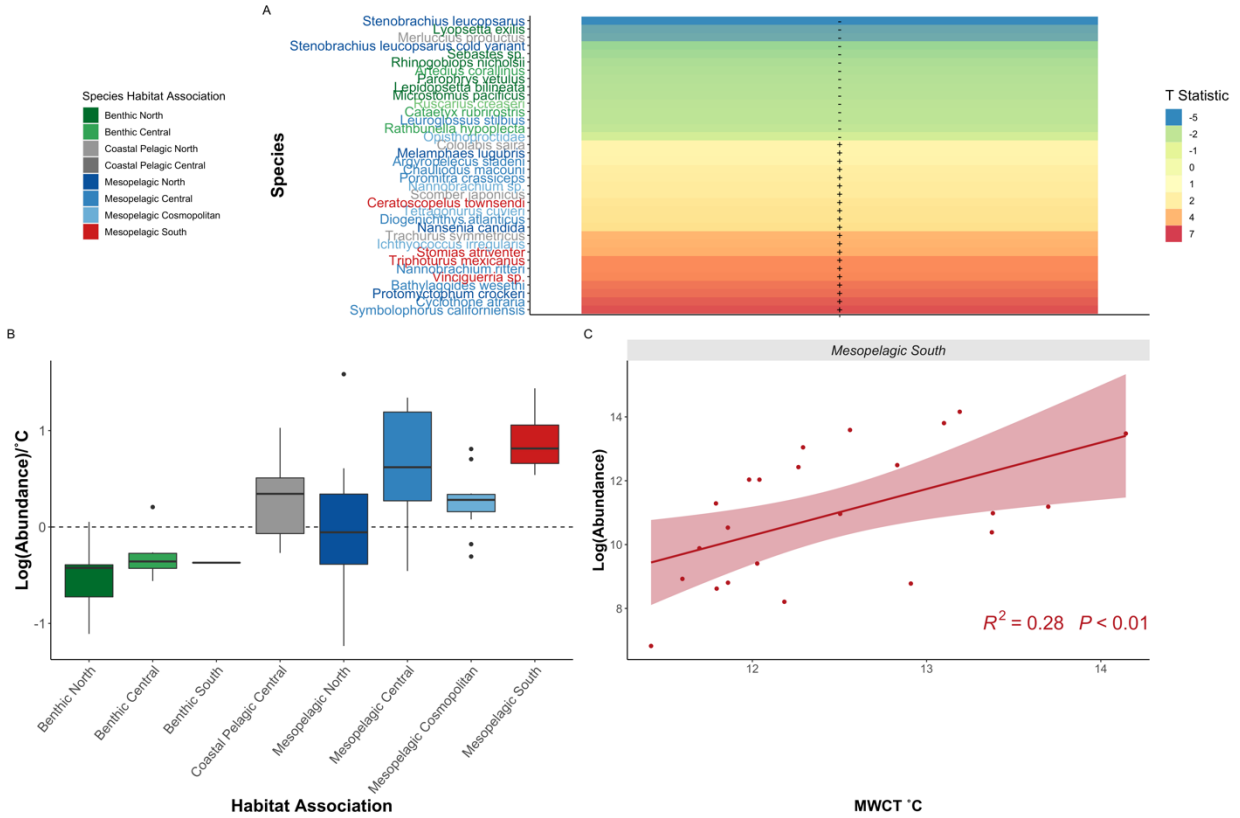


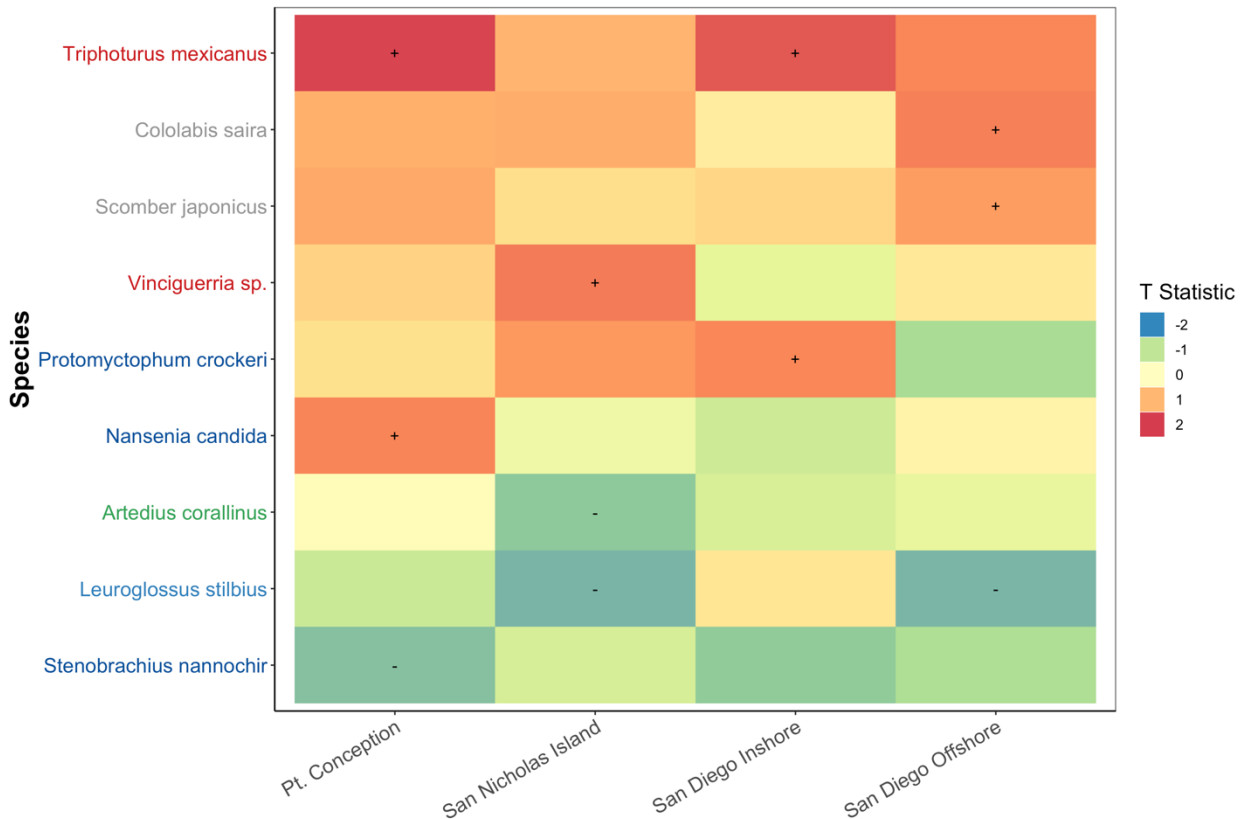
### Figure S7. Southern Oceanic Species Drive Fish Community Shifts

We capture changes in species biomass in response to MWCT, with Southern Mesopelagic species increasing in abundance with elevated temperature (A). T statistic (slope coefficient/standard error) from generalized linear models were calculated for each species across all stations. Only species with significantly different slopes (95% CI greater or less than zero) are plotted. Southern mesopelagic fishes were associated with increased temperature as indicated by the boxplots of all species-specific slopes from generalized linear models (B) and by the aggregated abundance relationship (C). In contrast, benthic species, as well as Northern Hake and Pacific Sardine abundances, were correlated with cooler temperatures.

601  
602

603  
604  
605  
606  
607  
608  
609  
610  
611  
612  
613  
614

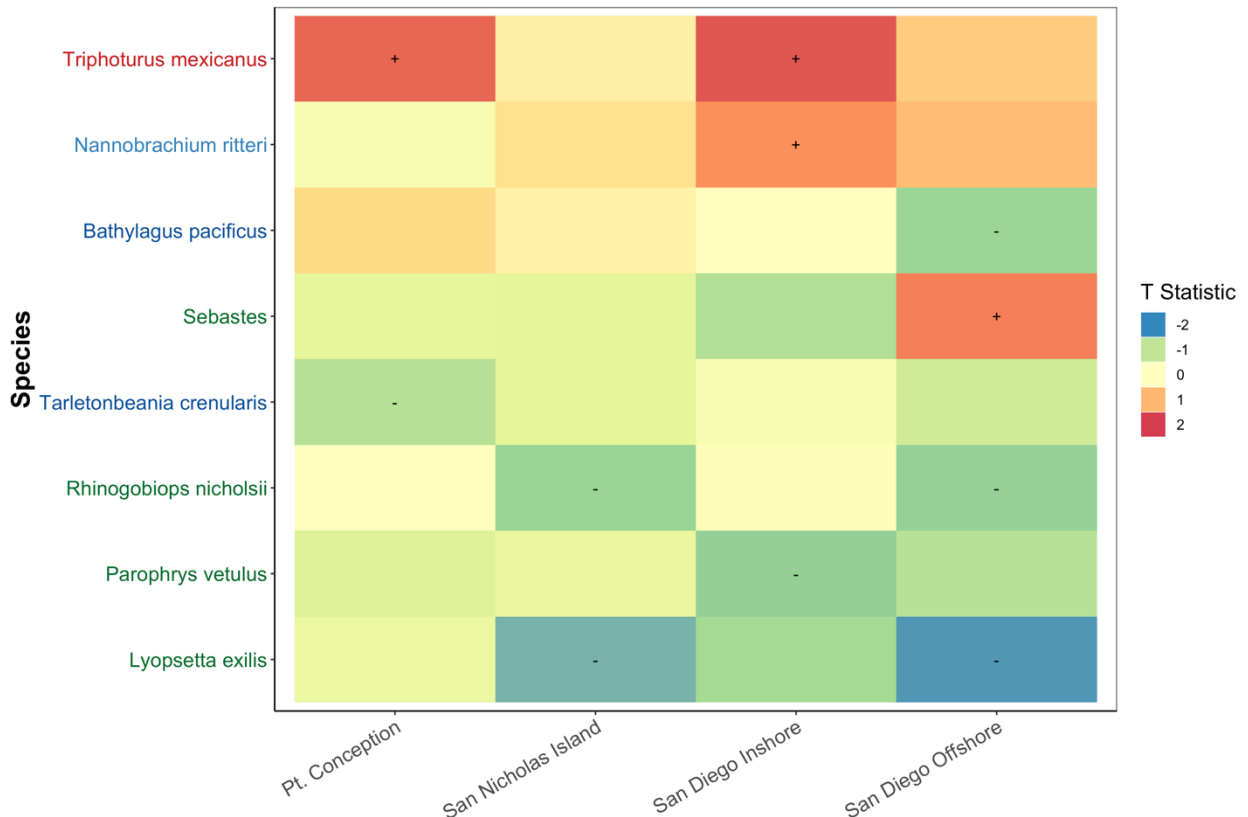
615  
616  
617



618

619 **Figure S8. Significant Species Occurrence and SST Correlations at each Station**

620 Occurrence of the Mexican lampfish (*Triphoturus mexicanus*) was positively correlated  
 621 with increased SST at the three northernmost stations. Generalized binomial mixed model  
 622 of occurrence versus SST was calculated for each species at each station. Only species  
 623 with significantly different slopes (95% CI greater or less than zero) are plotted. Colors  
 624 correspond to T statistic (slope coefficient/ standard error). Colors of species names  
 625 correspond to habitat associations described in Figure 2.



626

627

### Figure S9. Significant Species Occurrence and MWCT Correlations at each Station

628

Occurrence of the Mexican lampfish (*Triphoturus mexicanus*) was positively correlated

629

with increased MWCT at the three northernmost stations. Generalized binomial mixed

630

model of occurrence versus MWCT was calculated for each species at each station. Only

631

species with significantly different slopes (95% CI greater or less than zero) are plotted.

632

Colors correspond to T\_statistic (slope coefficient/ standard error). Colors of species

633

names correspond to habitat associations described in Figure 2.

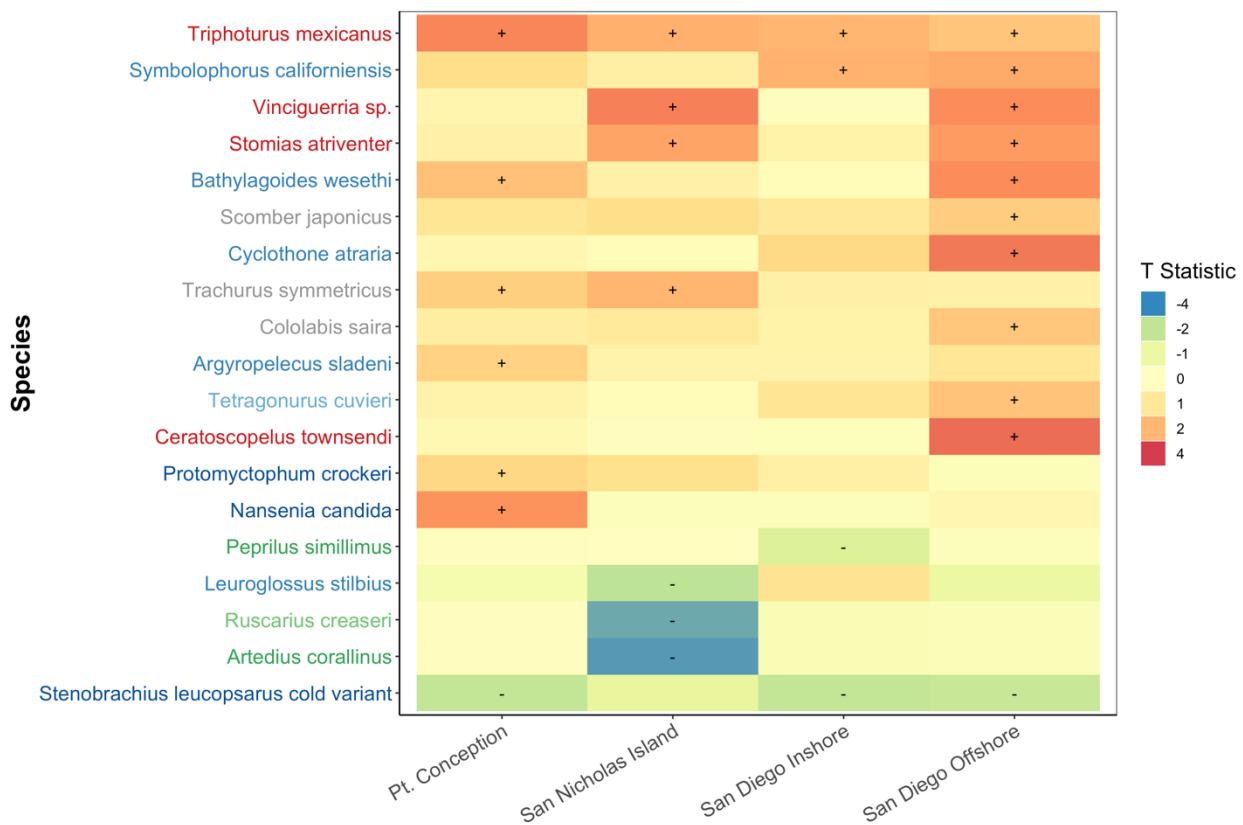
634

635

636

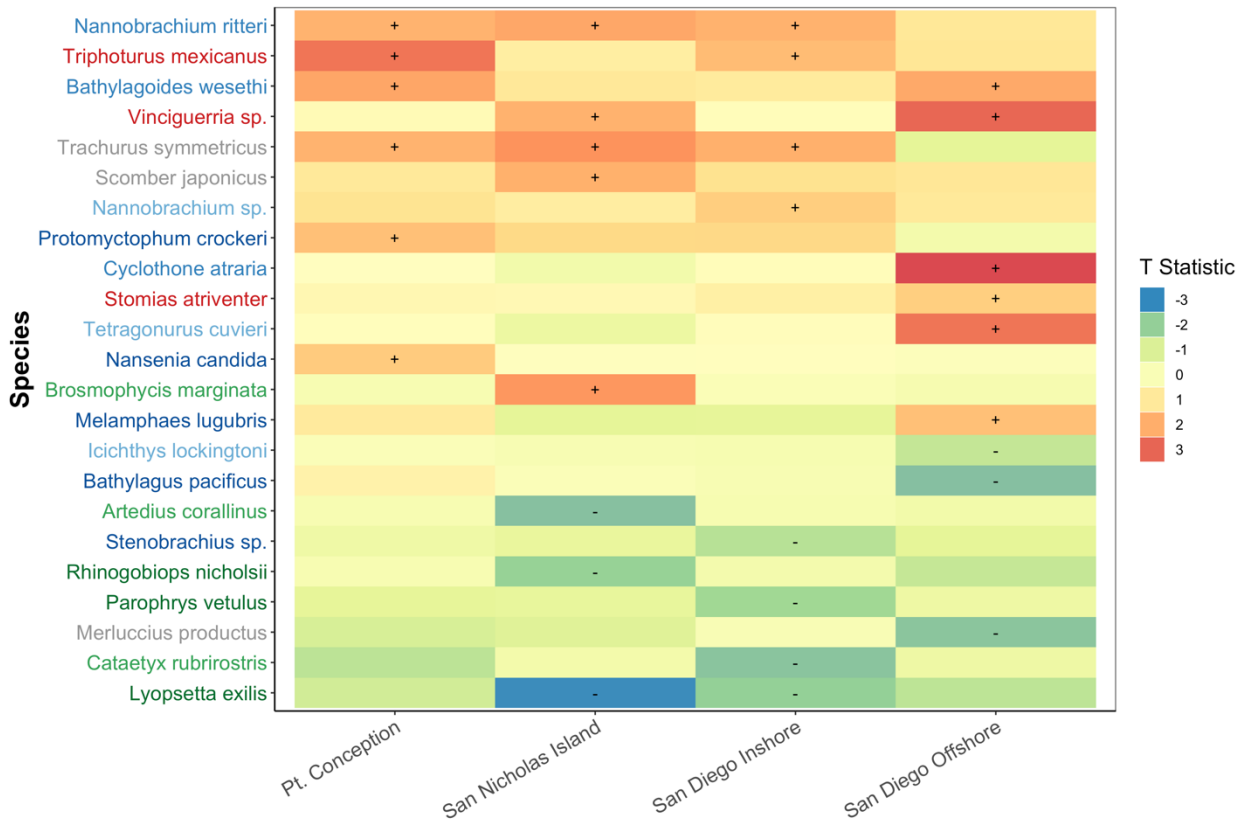
637

638



#### 641 **Figure S10. Significant Species Abundance and SST Correlations at each station**

642 The abundance of the Mexican lampfish (*Triphoturus mexicanus*) was positively  
 643 associated with increased SST at all stations. Likewise, the abundance of suite of  
 644 mesopelagic species including *Vinciguerra sp.*, *Symbolophorus californiensis*, and  
 645 *Stomias atriventer* among others increased with warmer SST. Generalized linear mixed  
 646 model of log (abundance) versus SST was calculated for each species at each station. Only  
 647 species with significantly different slopes (95% CI greater or less than zero) are plotted.  
 648 Colors correspond to T statistic (slope coefficient/ standard error). Colors of species  
 649 names correspond to habitat associations described in Figure 2.



650

651 **Figure S11. Significant Species Abundance and MWCT Correlations at each station**

652 The abundance of the Mexican lampfish (*Triphoturus mexicanus*) was positively  
 653 associated with increased MWCT at all stations. Likewise, the abundance of suite of  
 654 mesopelagic species including *Vinciguerra* sp., *Symbolophorus californiensis*, and  
 655 *Stomias atriventer* among others increased with warmer SST. Generalized linear mixed  
 656 model of log (abundance) versus MWCT was calculated for each species at each station.  
 657 Only species with significantly different slopes (95% CI greater or less than zero) are  
 658 plotted. Colors correspond to T statistic (slope coefficient/ standard error). Colors of  
 659 species names correspond to habitat associations described in Figure 2.

660

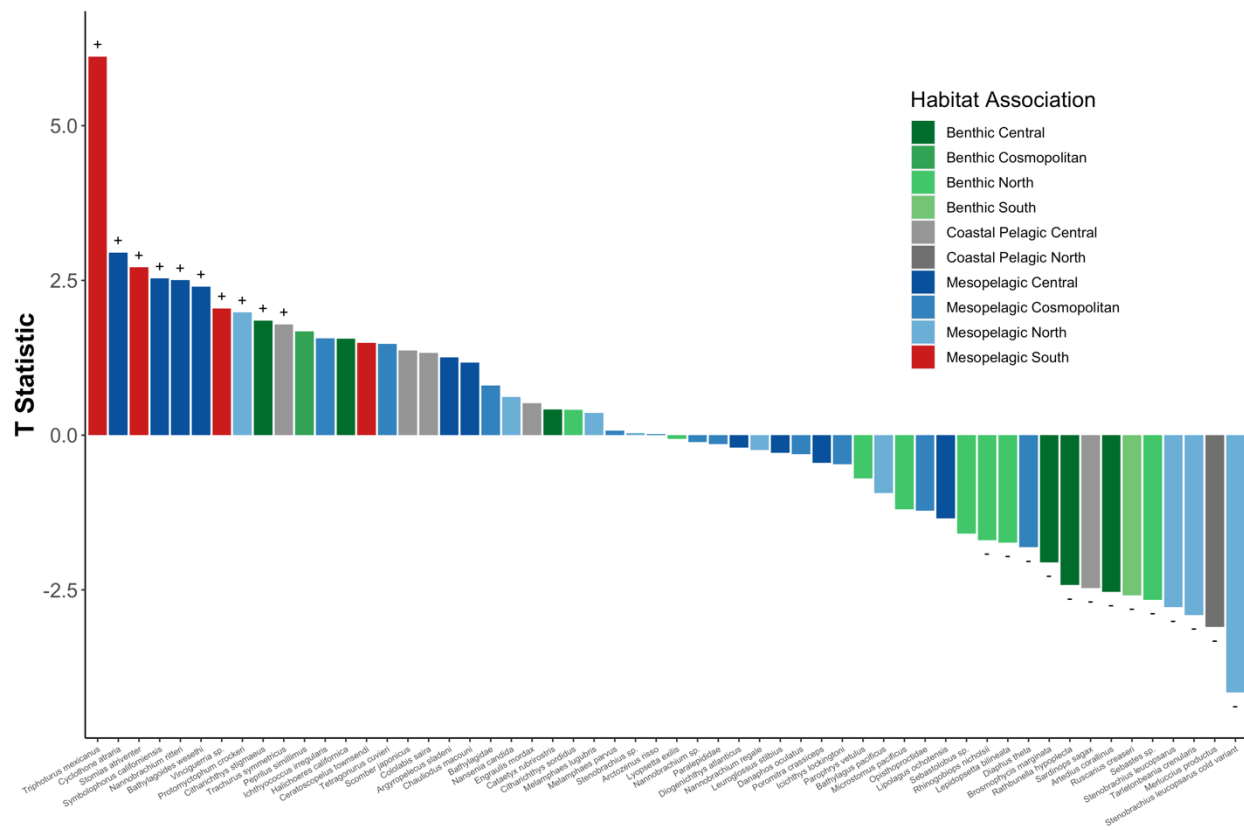
661

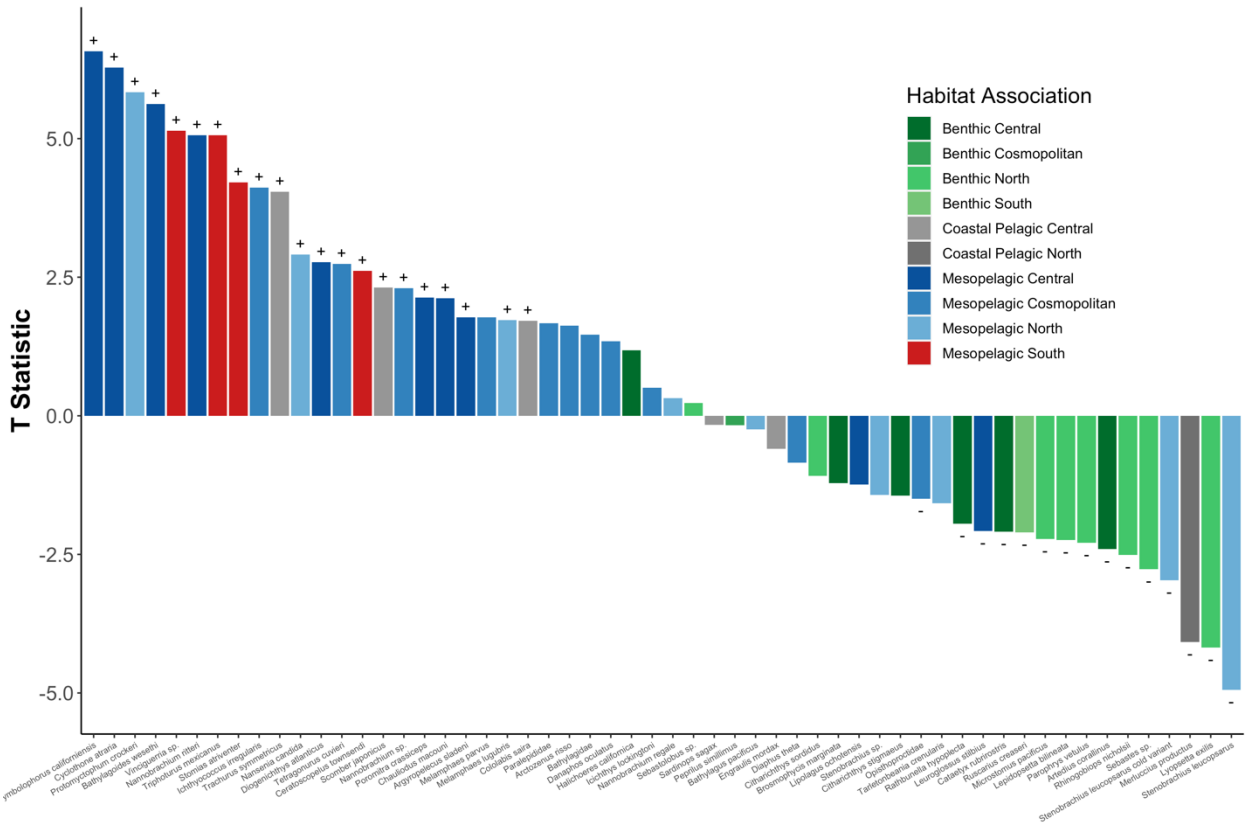
662

663

664

665





676

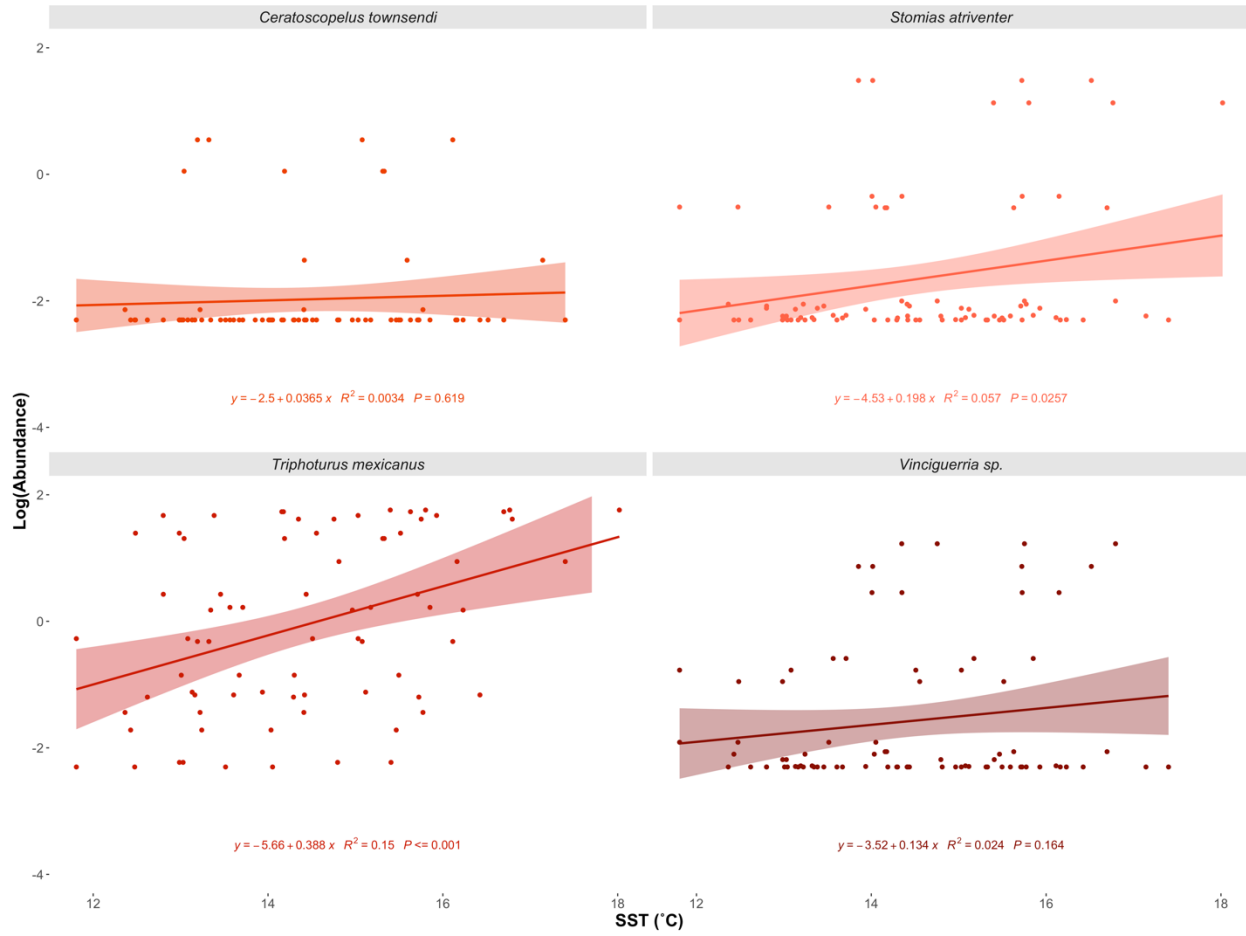
677 **Figure S13. Bar Plot of Significant Species Abundance and MWCT Correlations**678 **Across All stations**

679 The abundance of southern mesopelagic species increased with warmer temperatures  
 680 while fisheries targets like Pacific Sardine (*Sardinops sagax*) and North Pacific Hake  
 681 (*Merluccius productus*) decreased. Generalized linear mixed model of log (abundance)  
 682 versus SST was calculated for each species across all stations. Only species with  
 683 significantly different slopes (95% CI greater or less than zero) are plotted. Colors  
 684 correspond to T statistic (slope coefficient/ standard error).

685

686

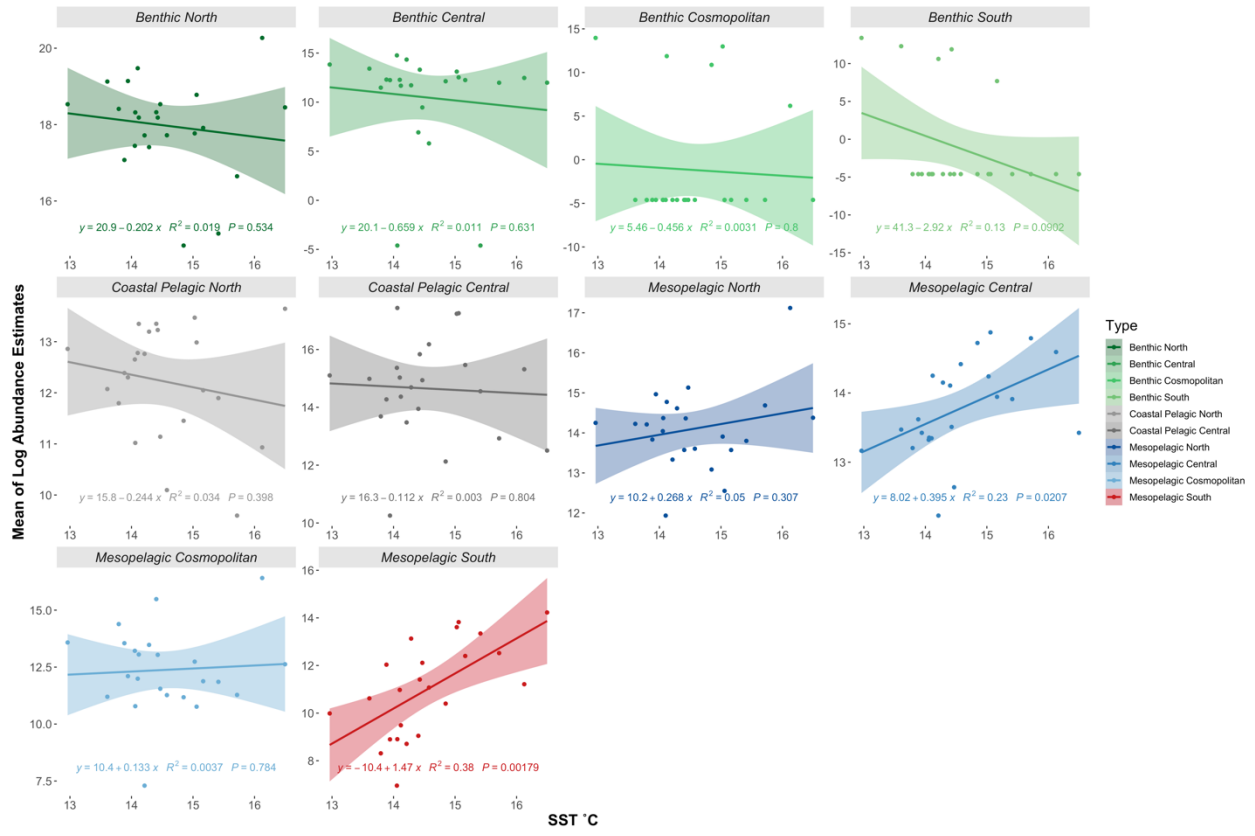
687



688

689 **Figure S14. Increased Abundance of Southern Mesopelagic Species with Higher  
690 SST**

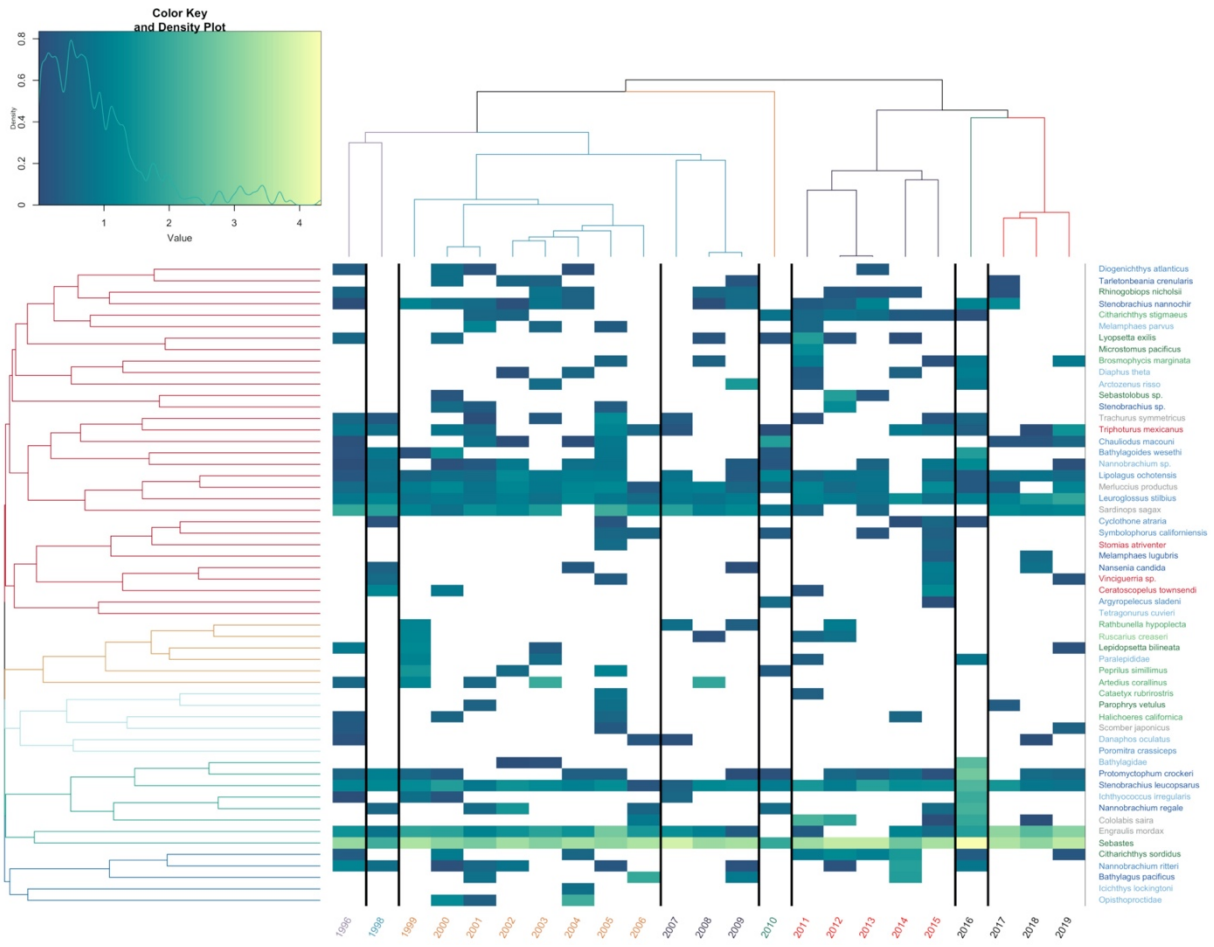
691 Species specific regressions of log (Abundance) vs. SST (°C). Three of the four  
692 southern mesopelagic species had significant positive associations between  
693 abundance and SST. Although not significant across all stations, the abundance of  
694 *Ceratoscopelus townsendi* significantly increased with higher SST at the San  
695 Diego Offshore station (Figure S7).



696

697 **Figure S15. Increased Abundance of Southern and Central Mesopelagic Species with  
698 Higher SST**

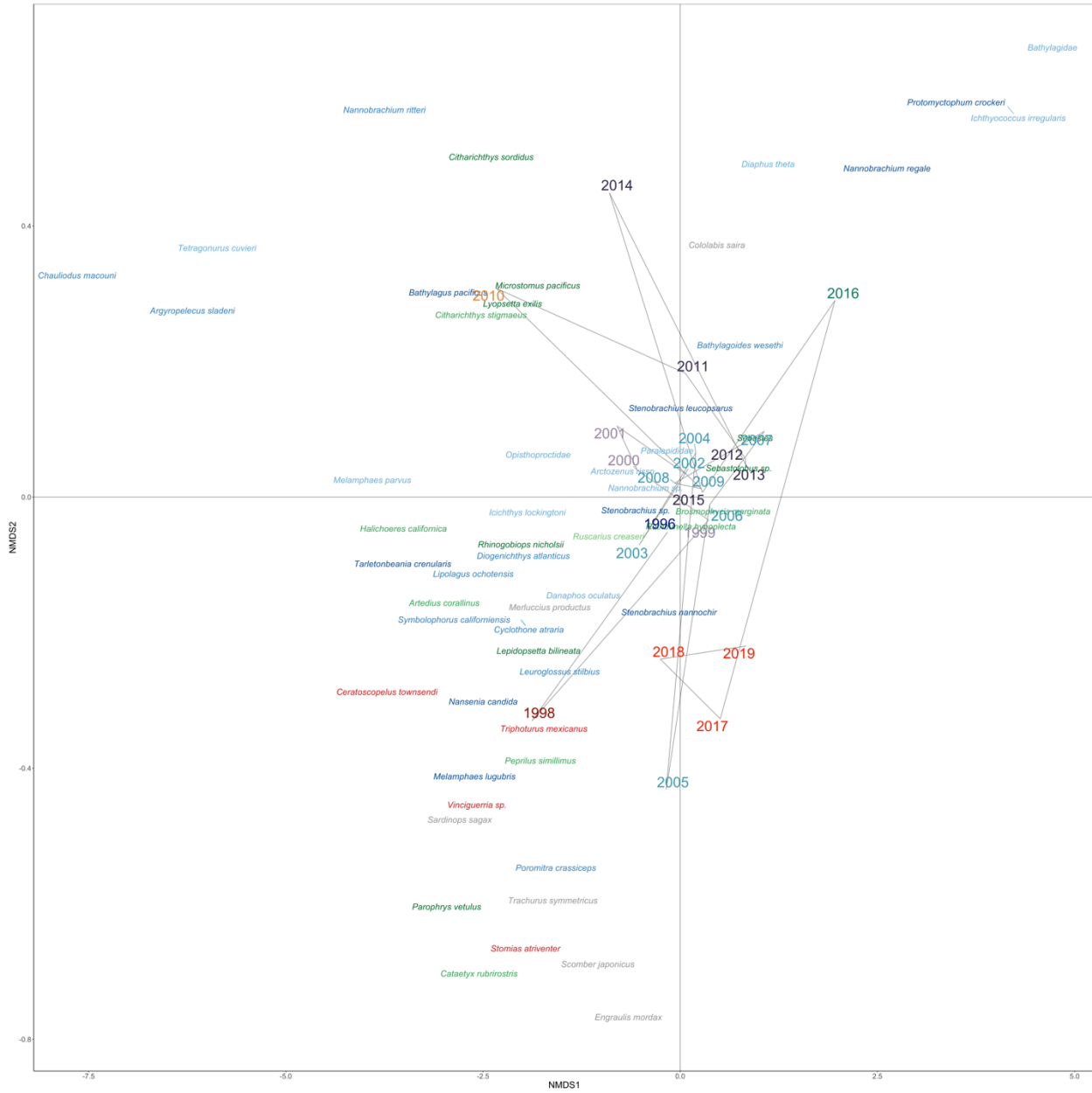
699 Abundances of each habitat association were summed at each station. Habitat association  
700 regressions were fit using sum total log (Abundance) vs. SST (°C).



701

## 702 **Figure S16. Heat Map of Abundances Over Time**

703 Northern Anchovy (*Engraulis mordax*) and rockfishes *Sebastodes* sp. dominated predicted  
 704 counts. Estimated abundance of each year, averaged across stations, plotted over time.  
 705 Years are color coded by chronological clustering. Species are grouped by hierarchical  
 706 clustering. Lighter colors indicate higher abundance, white is a lack of detection. Species  
 707 are color coded by habitat association matching Figure 1.



708

### Figure S17. NMDS Ordination of Species and Years

709

Fish assemblages changed across time with southern mesopelagics clustering with the

710

1998 and 2005 El Niños as well as 2017-2019 after the peak of the marine heat wave.

711

NMDS Ordination of Bray-Curtis dissimilarities calculated from summed abundance of

712

each year averaged across stations. Marine heatwave patterns are obscured by differential

713

onset and receding of the warming event across stations. Years are color coded by

714

chronological clustering ( $k = 8$ ). Species are color coded by habitat association matching  
Figure 2.

### Figure S18. NMDS Ordination of Species and Samples

719 Fish assemblages were strongly structured by stations, particularly the station just offshore  
720 of San Nicholas Island which had the highest abundance of *Sebastes* sp. NMDS  
721 Ordination of Bray-Curtis dissimilarities calculated from summed abundance of each year

averaged across stations. Marine heatwave patterns are obscured by differential onset and receding of the warming event across stations. Samples are color coded by station. Species are color coded by habitat association matching Figure 2.

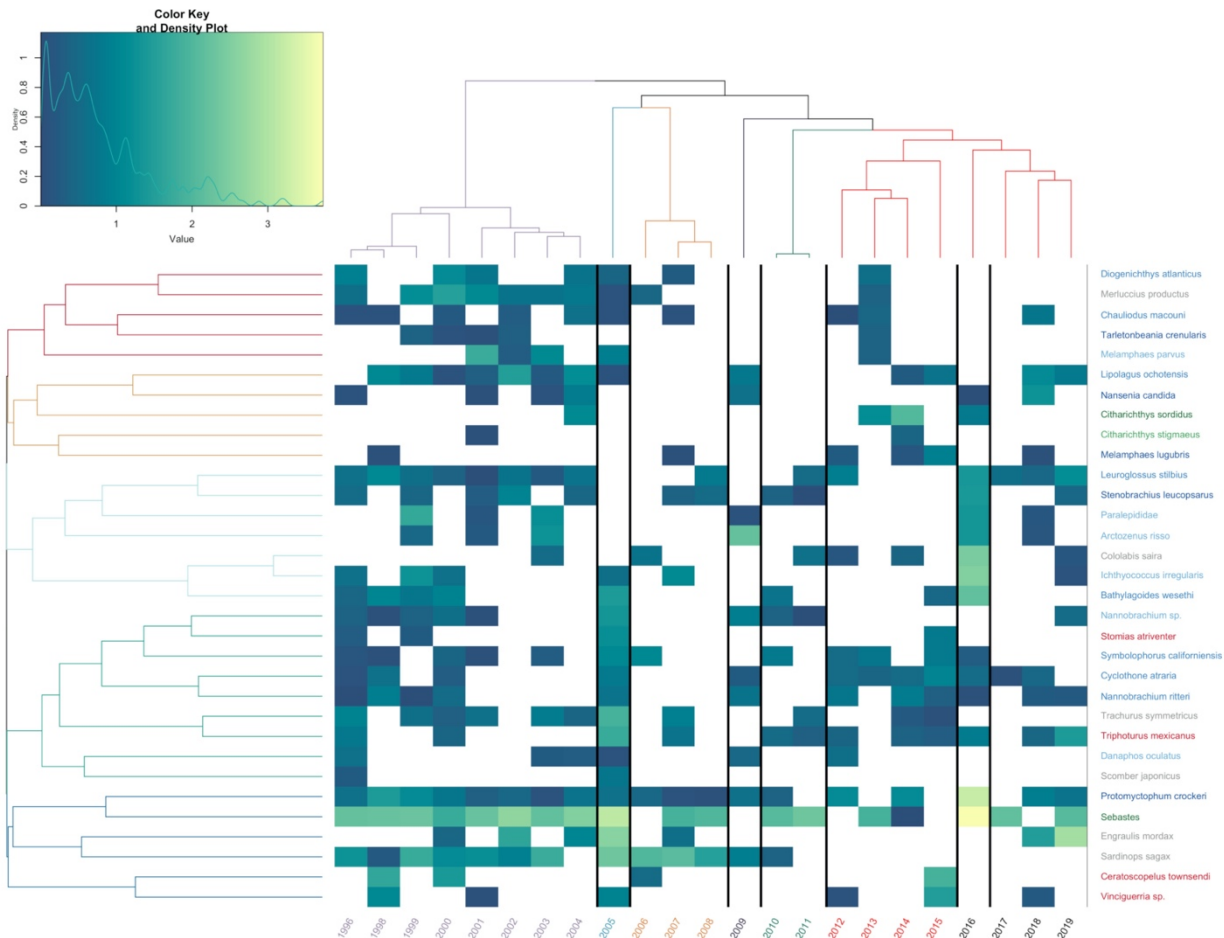
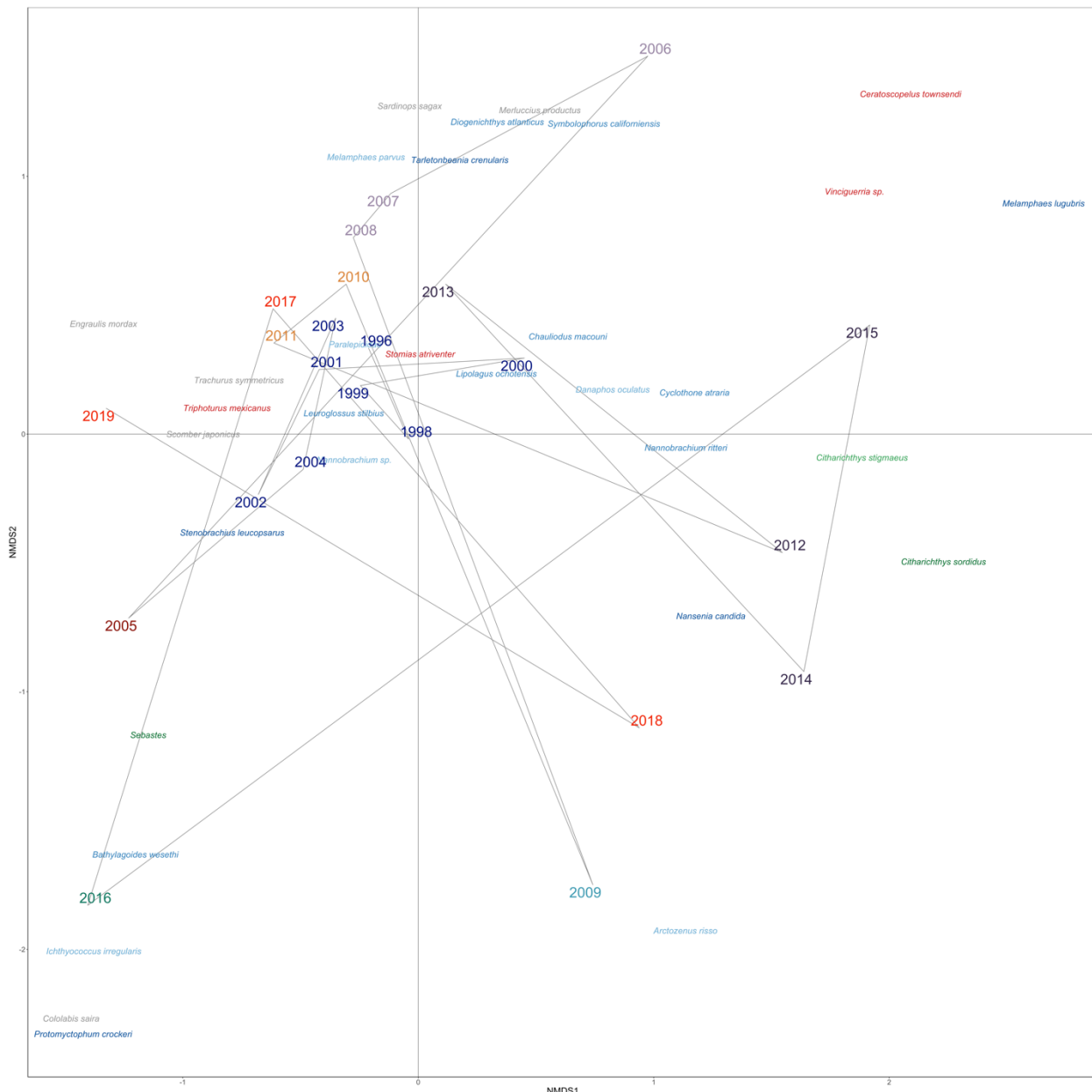


**Figure S19. Heat Map of San Diego Offshore Abundances Over Time**

Estimated abundance of each year plotted over time. Years are color coded by chronological clustering. Species are grouped by hierarchical clustering. Lighter colors indicate higher abundance, white is a lack of detection. Species are color coded by habitat association matching Figure 1.



731

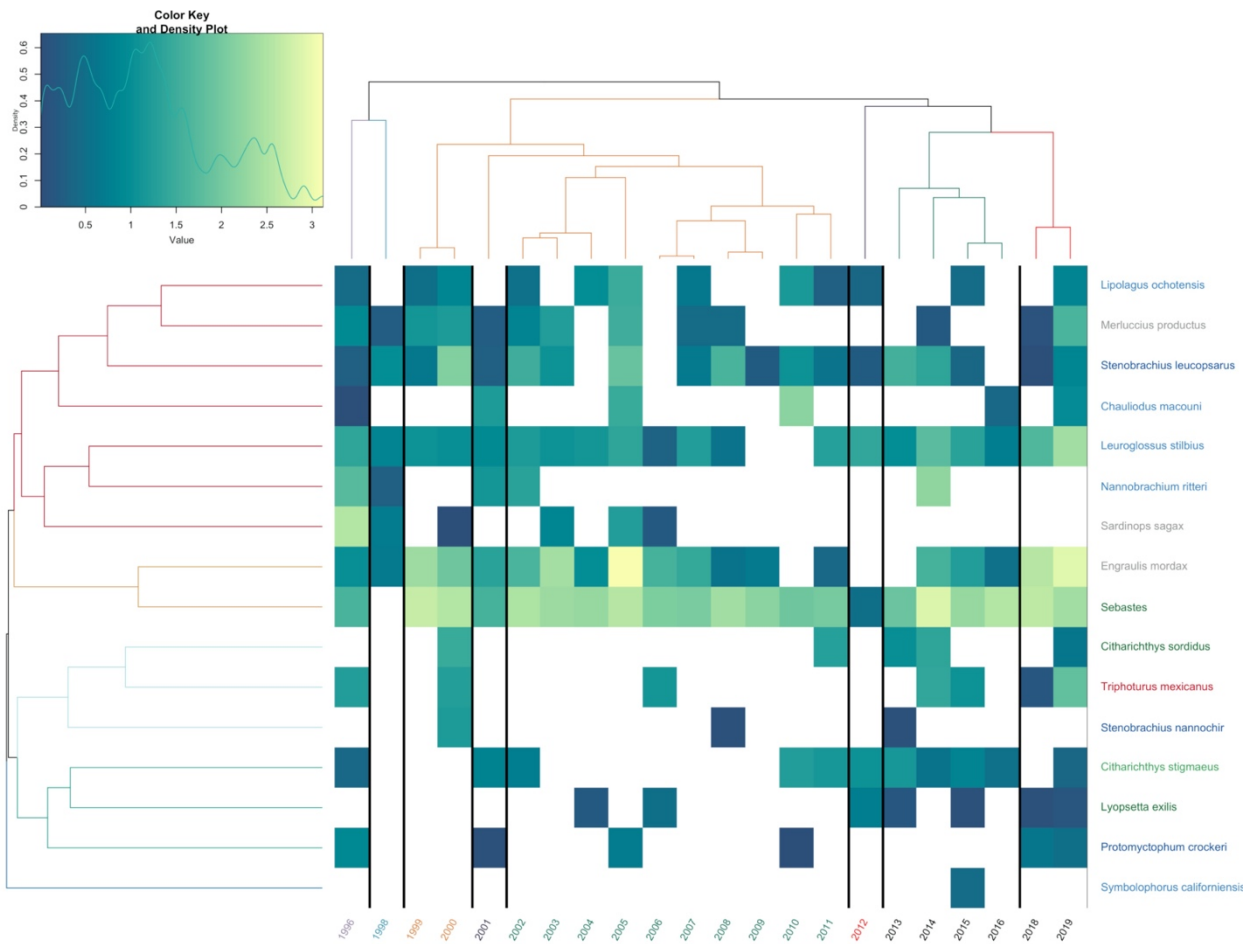
### 732 **Figure S20. NMDS Ordination of San Diego Offshore Species and Years**

733 NMDS Ordination of Bray-Curtis dissimilarities calculated from abundance of each year.

734 Years are color coded by chronological clustering ( $k = 8$ ). Species are color coded by

735

habitat association matching Figure 2.



736

### Figure S21. Heat Map of San Diego Inshore Abundances Over Time

737

Estimated abundance of each year plotted over time. Years are color coded by

738

chronological clustering. Species are grouped by hierarchical clustering. Lighter colors

739

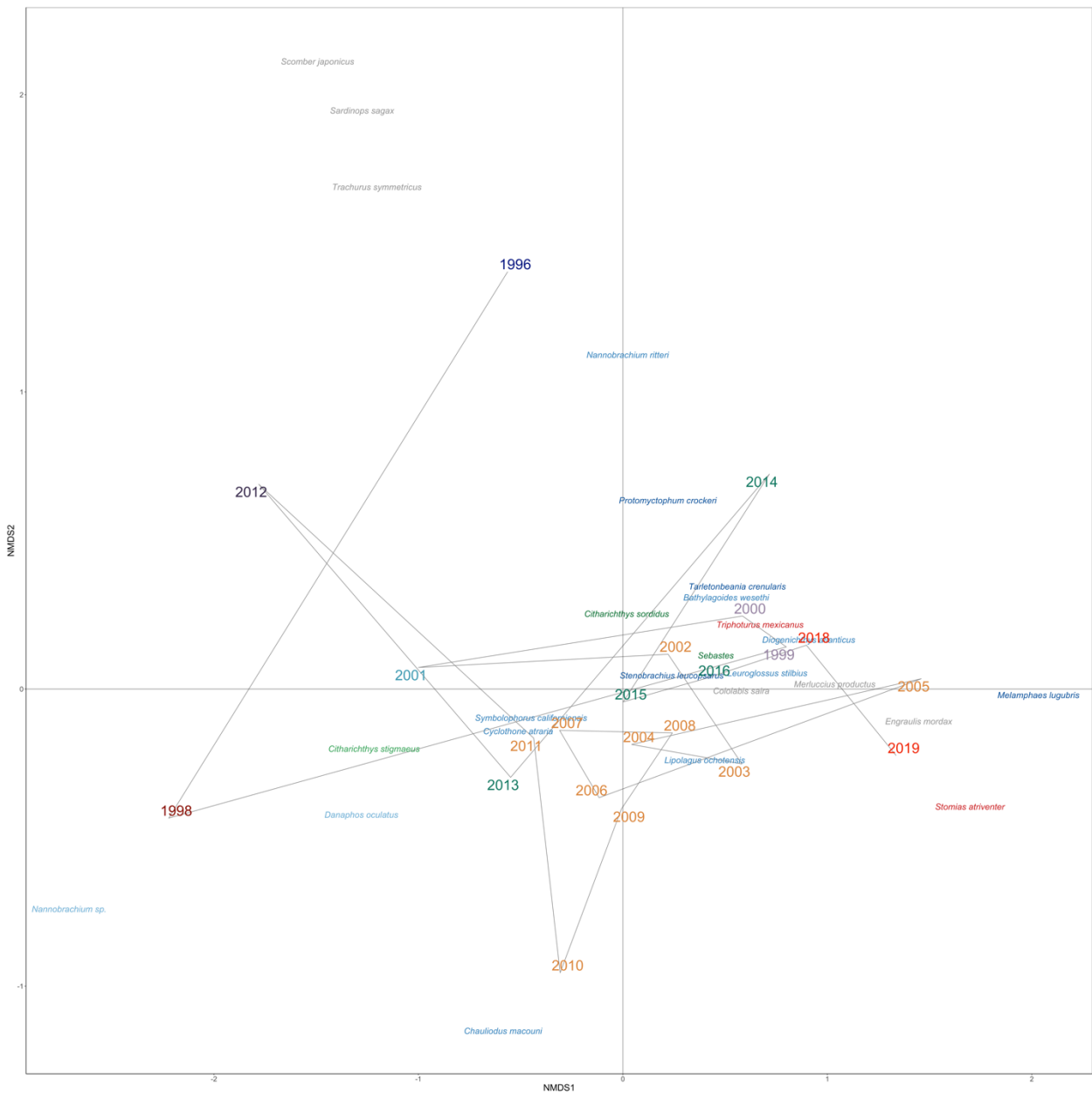
indicate higher abundance, white is a lack of detection. Species are color coded by habitat

740

association matching Figure 1.

741

742



743

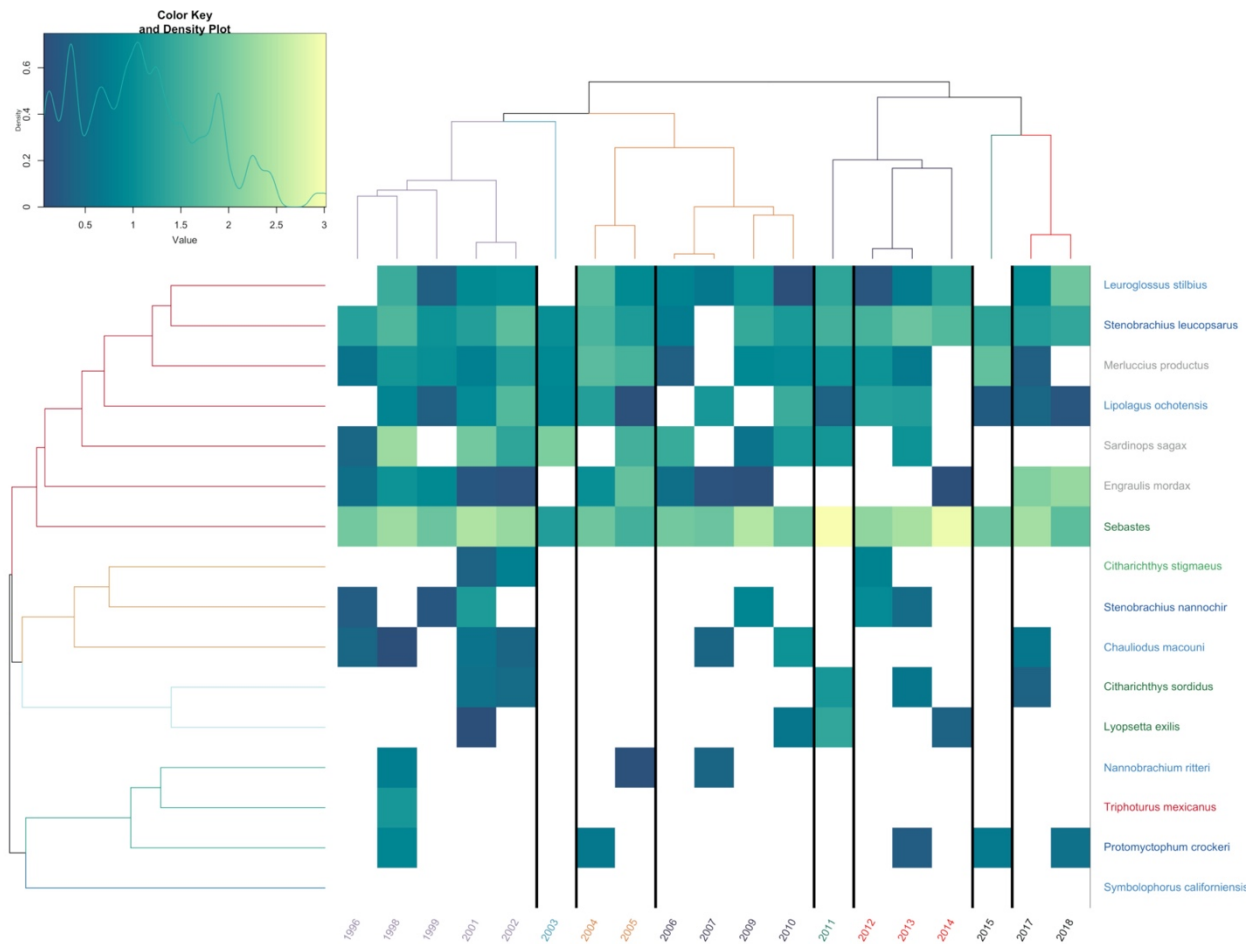
744 **Figure S22. NMDS Ordination of San Diego Inshore Species and Years**

745 NMDS Ordination of Bray-Curtis dissimilarities calculated from abundance of each year.

746 Years are color coded by chronological clustering ( $k = 8$ ). Species are color coded by

747

habitat association matching Figure 2.



748

### Figure S23. Heat Map of Pt. Conception Abundances Over Time

749

Estimated abundance of each year plotted over time. Years are color coded by

750

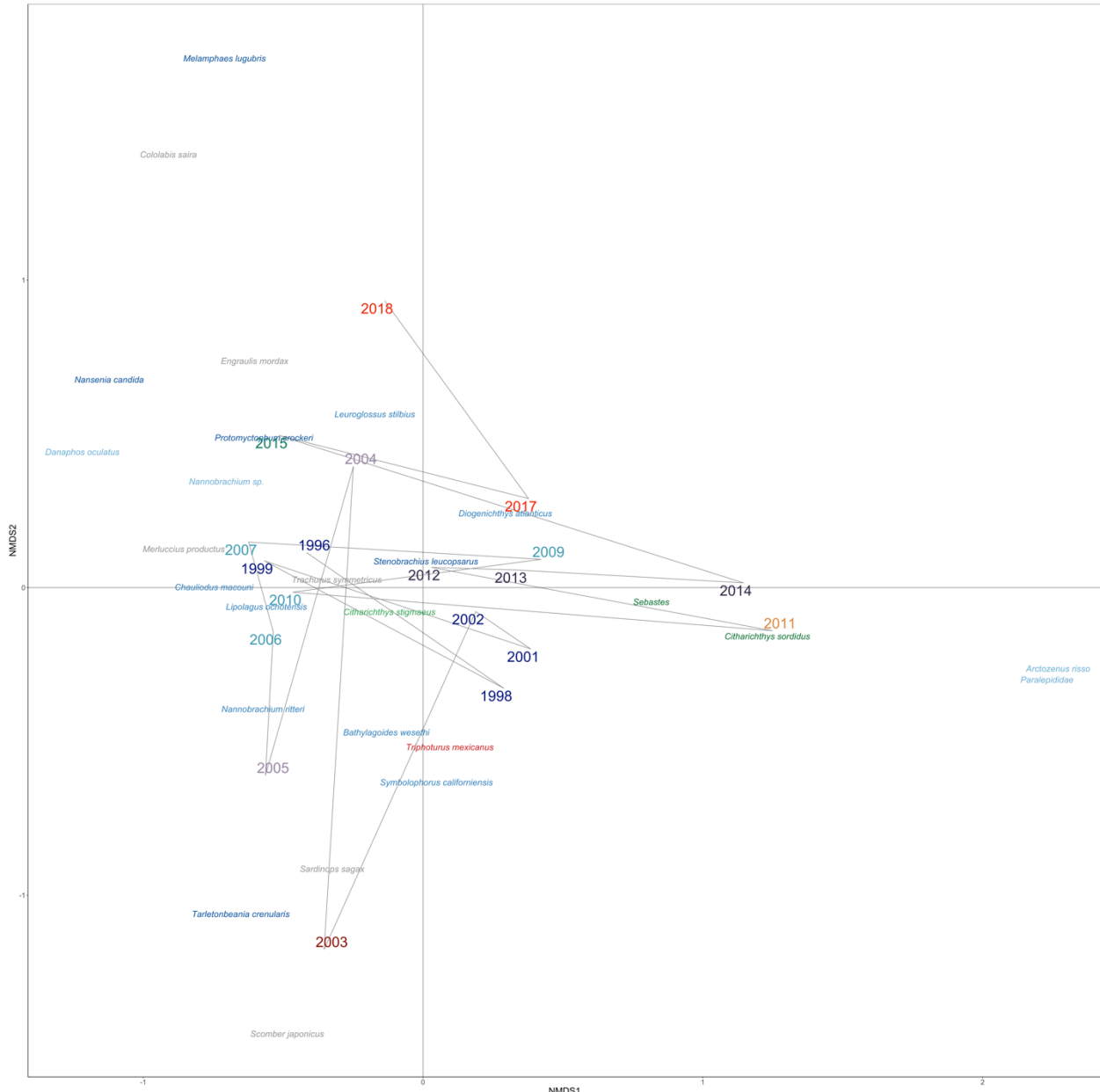
chronological clustering. Species are grouped by hierarchical clustering. Lighter colors

751

indicate higher abundance, white is a lack of detection. Species are color coded by habitat

752

association matching Figure 1.



754

## Figure S24. NMDS Ordination of Pt. Conception Species and Years

756

NMDS Ordination of Bray-Curtis dissimilarities calculated from abundance of each year.

757

Years are color coded by chronological clustering ( $k = 8$ ). Species are color coded by

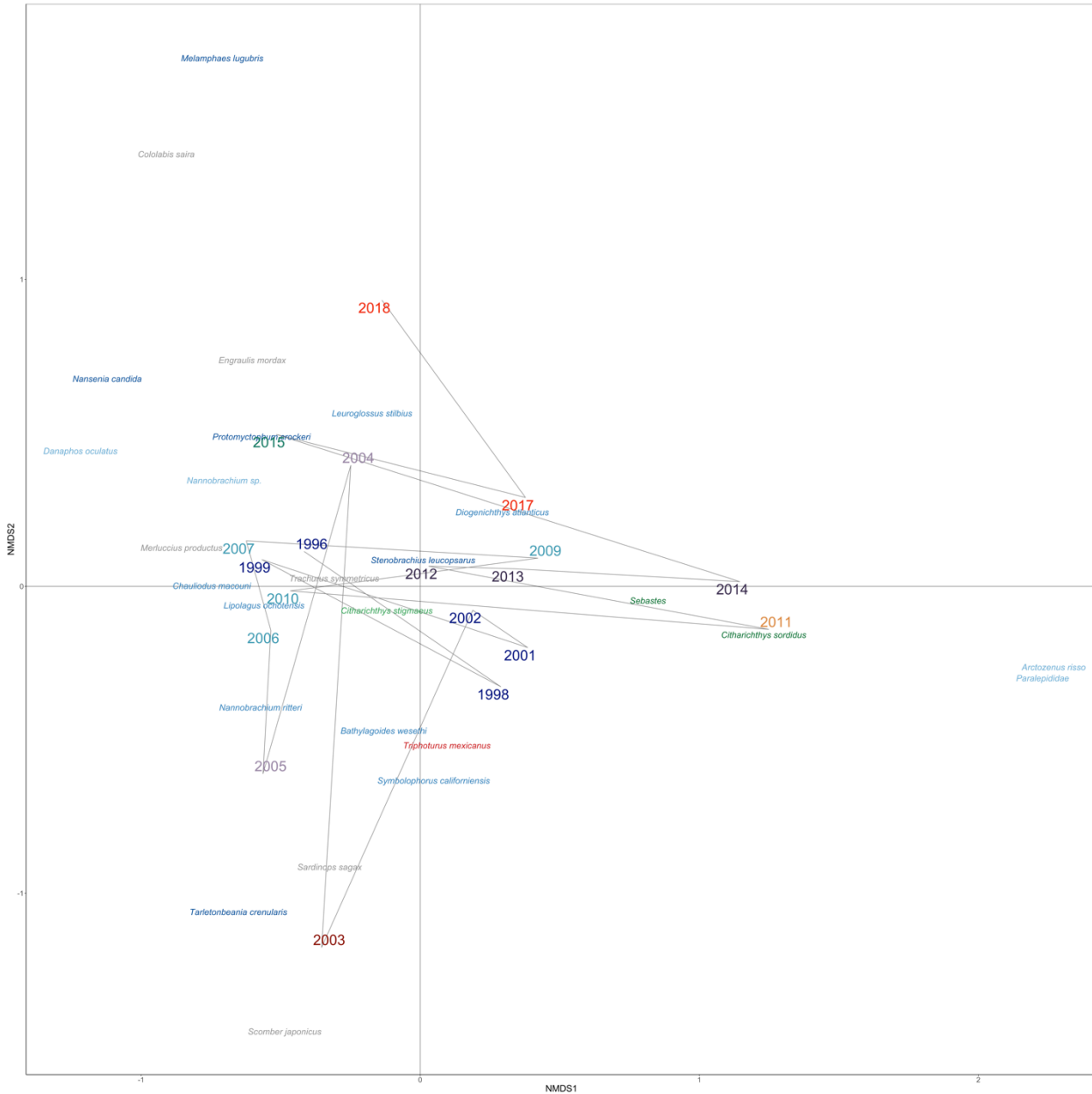
758

habitat association matching Figure 2.

759

## Figure S25. Heat Map of San Nicholas Island Abundances Over Time

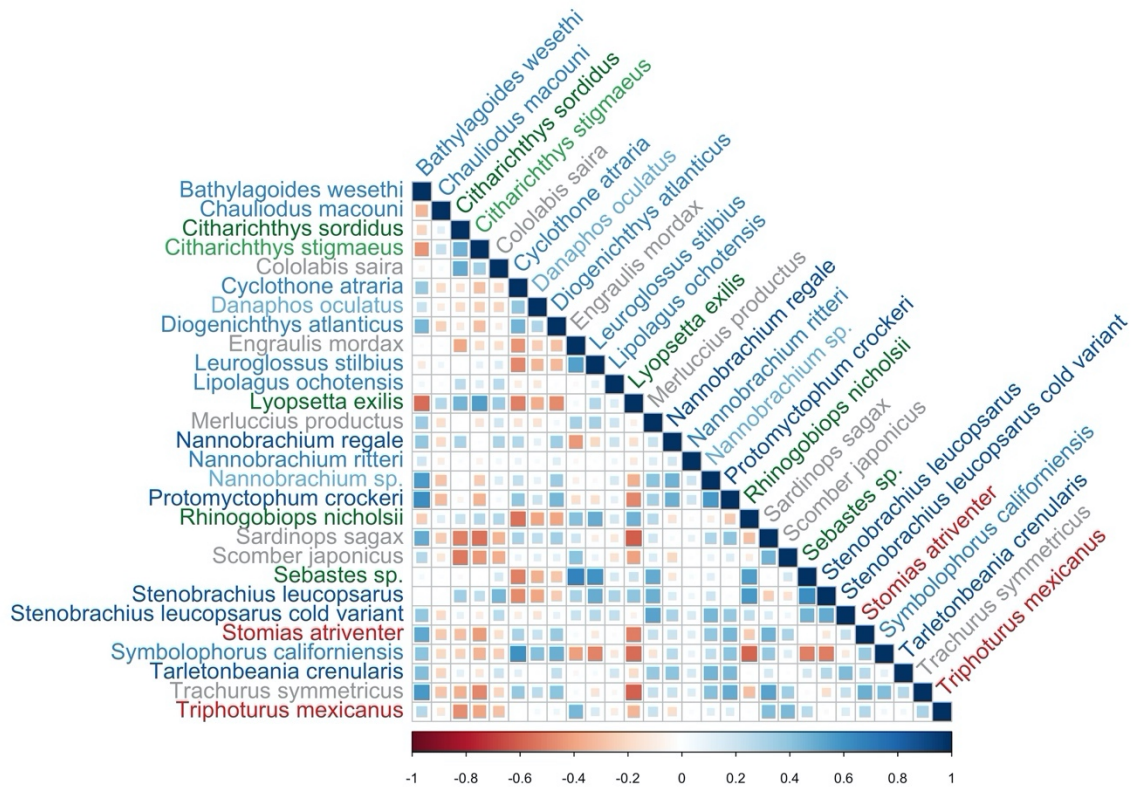
760 Estimated abundance of each year plotted over time. Years are color coded by  
 761 chronological clustering. Species are grouped by hierarchical clustering. Lighter colors  
 762 indicate higher abundance, white is a lack of detection. Species are color coded by habitat  
 763 association matching Figure 1.



764

765 **Figure S26. NMDS Ordination of San Nicholas Island Species and Years**

766 NMDS Ordination of Bray-Curtis dissimilarities calculated from abundance of each year.  
767 Years are color coded by chronological clustering (k =8). Species are color coded by  
768 habitat association matching Figure 2.  
769  
770  
771  
772  
773  
774

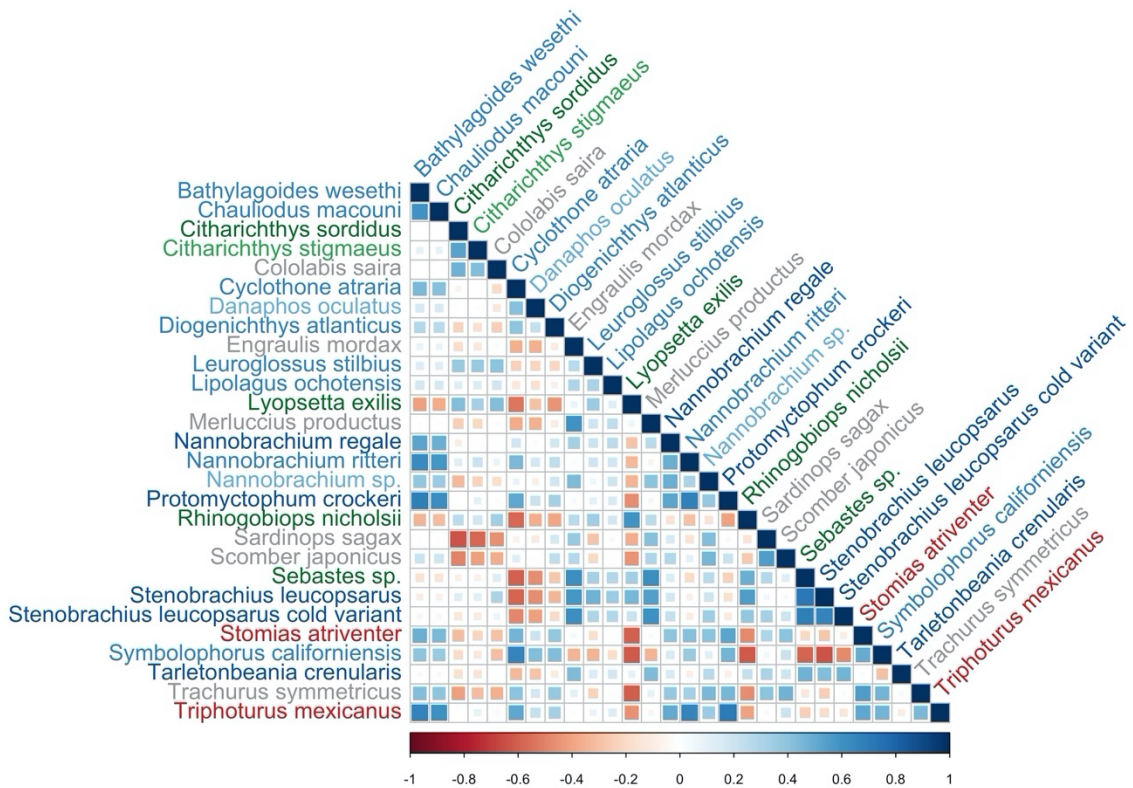


775

776 **Figure S27. Co-occurrence Patterns of Species Controlling for SST**

777 Benthic fisheries targets like sanddabs were negatively correlated with mesopelagic  
 778 species when controlling for SST. These results capture a strong benthic vs. pelagic  
 779 community dynamics when controlling for SST. We plot the correlation matrix of the  
 780 generalized linear latent variable model predictors across species. Species in blue correlate  
 781 are positively correlated with each other while species in red are negatively correlated.

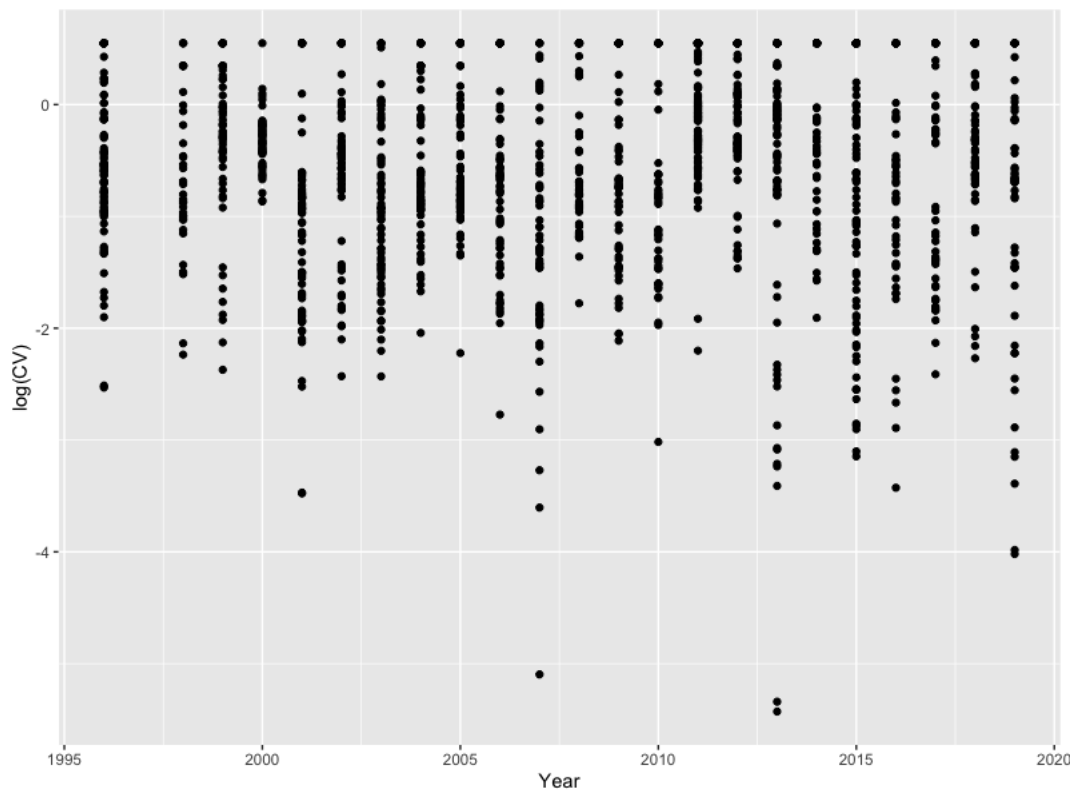
782 Strength of association is visualized by size of square. Species are color coded by habitat  
 783 association matching Figure 2.  
 784



785  
 786 **Figure S28. Co-occurrence Patterns of Species**  
 787 Fisheries targets like North Pacific Hake were negatively correlated with mesopelagic  
 788 species. We plot the correlation matrix of the generalized linear latent variable model

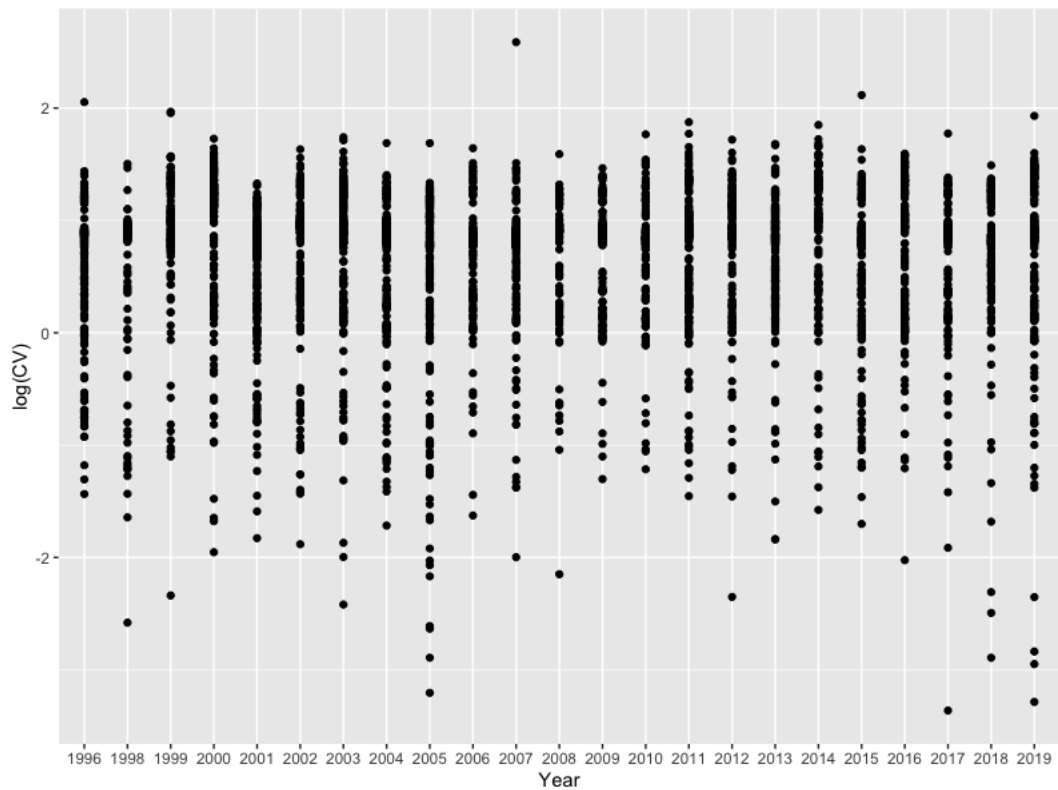
789 predictors across species. Species in blue correlate are positively correlated with each  
790 other while species in red are negatively correlated. Strength of association is visualized  
791 by size of square. Species are color coded by habitat association matching Figure 2.

792  
793



794  
795 **Figure S29. Stable Precision of Amplicon Abundance Over Time**

796 Here we measure the coefficient of variation (CV) of species-specific amplicons across  
797 three technical replicates. An increase in CV with the age of the sample would signal  
798 degradation; we see no such trend.



799

800

### Figure S30. Stable Precision of Abundance Estimates Over Time

801

Coefficient of variation of model estimates of abundance over time. We observe no evidence of change in precision over time.

803

## Supplement S2

Gold et al. 2021

### Model description of morphology and metabarcoding analysis of CALCOFI samples

#### Motivating models.

We use metabarcoding approaches outlined in Supplement S1 to produce amplicons from ethanol-preserved ichthyoplankton samples. Briefly, we generated amplicons using the MiFish 12S Universal Teleost primer set (1) on DNA extractions derived using the Qiagen DNeasy Blood and Tissue kit filtered ethanol-preserved. Each amplicon library was sequenced separately on an Illumina NextSeq. See Supplement S1 for full details.

We estimate that, for any species  $i$ , the number of sequenced amplicons is proportional to the fraction of DNA from that species in the PCR template (4). We note that here we use  $i$  to represent species, but can be more generalized to represent “molecular targets” or “amplicon sequence variants.” The amplicons produced during a PCR reaction are governed by the efficiency parameter  $\alpha_i$ , which is characteristic of the interaction between the particular primer set and each species being amplified. Thus, for any species  $i$ , the number of amplicons should be directly related to the efficiency of amplification and the starting concentration of DNA template such that

$$A_i = c_i(1 + \alpha_i)^{N_{PCR}} \quad (1)$$

where  $A_i$  is amplicon abundance,  $c_i$  is the true number of DNA copies in the reaction attributable to species  $i$ ,  $\alpha_i$  is the amplification efficiency (bounded on  $(0, 1)$ ), and  $N_{PCR}$  is a known constant (an integer giving the number of PCR cycles used in the reaction). If we could perfectly observe amplicons, the above equation would be all that we needed to relate the amplicons we observe and the biological value of interest,  $c_i$ , the true number of template DNA copies. Unfortunately standard PCR and sequencing technology does not allow for such direct observation. Due to  $N_{PCR}$  being a large number and  $\alpha_i$  typically being not close to 0, the number of amplicons expected for any species with  $c_i > 0$  is very, very large (e.g. with  $c_i = 2$ ,  $\alpha_i = 0.75$ , and  $N_{PCR} = 36$ ,  $A_i = 1.12 \times 10^9$ ) and there are typically many species being amplified simultaneously, producing  $10^{10}$  or more DNA copies in a single reaction. The actual number driven primarily by the  $\alpha$  values among species and  $N_{PCR}$ . This model assumes that PCR amplification has not approached saturation and therefore the PCR is still amplifying exponentially. We, and others (4), argue this assumption is valid because 1) the total concentration of DNA within a filtered ethanol sample is low ( $<1\text{ng}/\mu\text{L}$ ) and 2) the PCR reagents are supplied in excess and therefore are unlikely to be saturating the PCR. However, future models could be developed to account for a saturating PCR curve (5).

DNA sequencing machines do not read all of the copies from such a reaction; they read only a small fraction of the reads (on the order of  $10^6$  to  $10^7$  reads) (7). This subsampling changes what in eq. 1 appears to be a single-species process – each species being amplified independently – into a multi-species process; the number of amplicons observed for species  $i$  will depend upon both the amplicons produced for species  $i = 1$  and the amplicons produced for species  $i = 2, 3, \dots, I$  in the same reaction. Observations of amplicons are thus compositional data and need to be analyzed as such.

## Models for compositional data

We want to retain the data-generating structure from eq.1 as much as possible, so we develop a model for a single sample with many species. As above, let  $i$  index species with  $i = 1, 2, \dots, I$  and then we can write a deterministic equation for the number of amplicons observed in log-space as

$$\log(A_i) = \log(c_i) + N_{PCR} \log(1 + \alpha_i) + \log(\eta) \quad (2)$$

where the only new term is  $\eta$  which represents the proportion of reads observed from a given sampling run. Note that in this formulation  $\eta$  is a single value shared across all species and serves to scale the number of amplicons observed. Additionally we can rewrite the number of DNA copies in terms of proportional number of counts,  $\log(\beta_i) = \log(c_i) - \log(\sum_i c_i)$ . Note that the second term in this equation is a sum of the counts across all species, and so is a single shared value for all species. As such it can be absorbed into the value  $\eta$  that scales the overall abundance,

$$\log(A_i) = \log(\beta_i) + N_{PCR} \log(1 + \alpha_i) + \log(\eta) \quad (3)$$

This equation is appealing because it provides a process-oriented description of the biology of interest (the  $\beta$ s), a term for how PCR modifies our observation of the true abundance ( $N_{PCR} \log(1 + \alpha_i)$ ), and a term for how subsampling of DNA reads in the sequencing machine will adjust the number of amplicons observed  $\log(\eta)$ . This third term also links all of the single-species components to produce a multi-species model. It is important to note that while both eq. 2 and 3 use the term  $\eta$ , the interpretation and plausible range of this parameter are distinct in the two equations. In eq. 2,  $0 < \eta \leq 1$ , while in eq. 3  $\eta$  is not constrained to be less than 1 ( $\eta > 0$ ).

In practice, PCR and subsampling are not deterministic but random processes (7). Furthermore, we are rarely interested in results from a single sample but rather multiple samples collected across sites  $j$  and times  $t$ . We let  $\lambda_{ijtk}$  be the expected number of amplicons observed, with  $k$  indexing unique PCR reactions to account for the fact that there may be multiple individual PCR reactions for a single collected sample,

$$\log(\lambda_{ijtk}) = \log(\beta_{ijt}) + N_{PCR} \log(1 + \alpha_i) + \log(\eta_{jtk}) \quad (4)$$

Importantly,  $\alpha_i$  is assumed to be constant for each species among all sites, times, and PCR reactions (4). We incorporate stochasticity by allowing the number of observed amplicons to vary from the deterministic mean by specifying the observed values as following a negative binomial distribution,

$$Y_{ijk} \sim \text{NegativeBinomial}(\lambda_{ijtk}, \phi) \quad (5)$$

$$\phi = \exp[\tau_0 + \tau_1 \log(\lambda_{ijtk})] \quad (6)$$

where the expected value and variance of  $Y_{ijk}$  are  $E[Y_{ijk}] = \lambda_{ijtk}$ , and  $Var[Y_{ijk}] = \lambda_{ijtk} + \frac{\lambda_{ijtk}^2}{\phi}$ , respectively.

Note that we allow for the scale parameter  $\phi$  to vary with the predicted mean, this allows for the amount of dispersion in the negative binomial to shift with changing predictions. For our datasets, this allows dispersion to be large when  $\lambda$  is small and decrease as  $\lambda$  increases.

By itself, this model has substantial identifiability problems; in the absence of additional information, it is not possible to estimate the  $\beta$  and  $\alpha$  parameters. In the next section we discuss how to integrate data from amplicon sequencing as well as other data sources to make the parameters identifiable.

## Application to the CalCOFI Dataset

At each CalCOFI station, an oblique bongo-net tow is conducted from 210 m to the surface with the starboard side preserved in buffered formaldehyde and the port side preserved in buffered ethanol-preserved (See Supplemental S1 for more details)(8). Manual counts of ichthyoplankton were quantified using microscopy to identify species abundance from formaldehyde-preserved samples. Metabarcoding was conducted on the ethanol preserved side; consequently, we expect the contents of the paired samples to differ slightly as a function of sampling stochasticity. Counts of larvae/juveniles were done once for each jar.

The manual counts provide extra information that enable us to estimate the confounded parameters from the metabarcoding. Specifically, for each sampled station, we have two sets of observed data: 1) counts of larval/juvenile fishes for each taxon from the formaldehyde jars ( $Z_{ijt}$ ; indexes as above) and 2) counts of amplicons for each taxon from ethanol jars ( $Y_{ijtk}$ ). These observed data arise from a common (but unobserved) biomass for each species at each station-year combination ( $\gamma_{ijt}$ ; a latent (unobserved) variable).

We assume that the data are counts for each species in each sample,  $Z_{ijt}$ , derived from the true density of each species  $\gamma_{ijt}$ , the fraction of total specimens counted in each vial,  $P_{jt}$ , and the volume of water filtered for that station relative to a standard volume,  $V_{jt}$ ;  $V_{jt} \approx 1$  for most samples,  $V_{jt} < 1$  indicates a smaller volume of water was sampled.

$$Z_{ijt} \sim \text{Poisson}(\theta_{ijt}) \quad (7)$$

$$\log(\theta_{ijt}) = \log(\gamma_{ijt}) + \log(P_{jt}) + \log(V_{jt}) \quad (8)$$

We consider  $\beta_{ijt}$  to be the true proportion of biomass at a given station-year for each taxon  $i$ ,  $\beta_i = \frac{\gamma_{ijt}}{\sum_i \gamma_{ijt}}$ .

## Joint Model for Counts and Amplicons

To combine our information from the manual counts and metabarcoding, we need to recognize that our observations ( $Y_{ijtk}$  and  $Z_{ijt}$ ) are linked together by a common variable ( $\gamma_{ijt}$ ) and thus we can model them jointly (9). We represent the amplification process using equation 5 and 6 above (amplicons were sequenced in triplicate reactions for each jar). The manual count are modeled as in equations 7 and 8.

Our model assumes the fraction of template DNA in each sample is proportional to the counts of individual species' larvae in each paired jar (4). Moreover, we assume that in each sample there is template DNA from species that are uncounted, unidentifiable, or otherwise unobserved (7). In practice, this DNA might derive from stochastic sampling between each side of the bongo net, excreted waste, stray tissue, cells, or microscopic genetic material extracted along with the visible larvae.

### Dealing with the fact that not all methods see the same species

The above is sufficient if all of the species identified by morphological counts are identical to the species identified by the genetic methods. But this is often not the case; some larvae are not separable to species based on morphology and some species are not separable to species based on a single genetic primer. Furthermore, some species do not amplify at all in the PCR ( $\alpha_i \approx 0$ ). To accommodate non-overlapping sets of species among sampling methods we introduce a new variable,  $\gamma_{Mijt}$ , which specifies the true ( $M$  is for "main") density of species  $i$  at site  $j$  and time  $t$ . We assume that there is a mapping between this main density and the density observed by each sampling method. Specifically, we assume the species in the main list maps uniquely onto no more than one taxonomic group in each observation method, but multiple main species can map onto a single group for each observation method. For example, if the observation of larval counts identified as a specimen as *Sebastes* sp., we assume this may map onto one or more specific taxa (e.g., *Sebastes paucispinis*) in the main list, but conversely, *Sebastes paucispinis* on the main list may not map to more than one entity identified by each observation method.

We can construct a mapping matrix,  $\mathbf{M}_{MS}$ , that transforms the species in the main list,  $\gamma_M$  (a vector of length  $I_M$ , the number of true species in the sample) into the species grouping observed by sampling method

$S$ ,  $\gamma_S$  (a vector of length  $I_S$ , the number of groups observed by method  $S$ ). We drop the  $j$  and  $t$  subscript because this mapping does not depend on the identity of the community being sampled. Then,

$$\gamma_S = \mathbf{M}_{MS} \gamma_M \quad (9)$$

$\mathbf{M}_{MS}$  is a  $I_S$  by  $I_M$  matrix.

For example, if there are four species in the true community and method  $S$  only observes three groups, the matrix  $\mathbf{M}_{MS}$  could look like this

$$\mathbf{M}_{MS} = \begin{bmatrix} 1 & 0 & 0 & 0 \\ 0 & 1 & 0 & 1 \\ 0 & 0 & 1 & 0 \end{bmatrix} \quad (10)$$

This might happen if species 2 and species 4 (columns 2 and 4, respectively) were from the same genus and the PCR primer from method  $S$  can only resolve those two species at the genus level. To provide a further example, take an invented community of four species with  $\gamma_M = \{1, 15, 6, 7\}$  individuals in the community. The true community as observed through method  $S$  would be

$$\gamma_S = \mathbf{M}_{MS} \gamma_M \quad (11)$$

$$\begin{bmatrix} 1 \\ 22 \\ 6 \end{bmatrix} = \begin{bmatrix} 1 & 0 & 0 & 0 \\ 0 & 1 & 0 & 1 \\ 0 & 0 & 1 & 0 \end{bmatrix} \begin{bmatrix} 1 \\ 15 \\ 6 \\ 7 \end{bmatrix} \quad (12)$$

and so  $\gamma_S$  is a linear combination of the true community. Of course there is no requirement that elements of  $\gamma_M$  be integers, but that makes the above example easy and transparent.

It is easy to incorporate this added complexity into the models in the previous section. If we assign method  $S$  to be manual counts and  $W$  to be the Mifish PCR primer, we need to construct a main list of species to define  $\gamma_M$  and build two mapping matrices,  $\mathbf{M}_{MS}$  and  $\mathbf{M}_{MW}$  that determine which species or species-groups are observed by each method. We can then add an additional subscript for each additional method and use the same form as above. For example,

$$\log(\theta_{Sijt}) = \log(\gamma_{Sijt}) + \log(P_{Sjt}) + \log(V_{Sjt}) \quad (13)$$

$$\log(\lambda_{Wijtk}) = \log(\beta_{Wijt}) + N_{W,PCR} \log(1 + \alpha_{Wi}) + \eta_{Wjtk} \quad (14)$$

And with additional sampling methods, we can make different mappings from the true abundance to the observations of each method.

### Estimation and Identifiability

We developed and fit the above model in a Bayesian framework using the Stan language, as implemented in *RStan* (11). All code is available as supplementary material. Table S2.1 provide prior distributions used in the model.

We ran five MCMC chains with 1,000 warmup and 4,000 sampling iterations. We retained every other MCMC sample. We initiated each chain at randomly determined starting values. The model converged ( $\hat{R} < 1.01$ ; Gelman-Rubin diagnostics) and had no divergent transitions. We performed standard posterior predictive checks to assess model fit.

Table S2.1: Prior and parameter descriptions for the Stan Model.

Parameter & Prior	Description
$\alpha_i \sim Beta(1, 1)$	Amplification efficiency for species $i$
$\log(\gamma_{Mijt}) \sim Normal(0, 4)$	True biomass of each species at each site-year
$\log(\eta_{jtk}) \sim Normal(-4, 4)$	Estimated offset for each PCR reaction at each site-year
$\tau_0 \sim Normal(0, 2)$	Negative Binomial shape parameter intercept
$\tau_1 \sim Normal(0, 2)$	Negative Binomial shape parameter slope

## References

1. M. Miya, Y. Sato, T. Fukunaga, T. Sado, J. Poulsen, K. Sato, T. Minamoto, S. Yamamoto, H. Yamanaka, H. Araki, others, MiFish, a set of universal PCR primers for metabarcoding environmental DNA from fishes: Detection of more than 230 subtropical marine species. *Royal Society open science*. **2**, 150088 (2015).
2. R. P. Kelly, A. O. Shelton, R. Gallego, Understanding PCR processes to draw meaningful conclusions from environmental DNA studies. *Scientific reports*. **9**, 1–14 (2019).
3. J. D. Silverman, R. J. Bloom, S. Jiang, H. K. Durand, S. Mukherjee, L. A. David, Measuring and mitigating PCR bias in microbiome data. *BioRxiv*, 604025 (2019).
4. M. R. McLaren, A. D. Willis, B. J. Callahan, Consistent and correctable bias in metagenomic sequencing experiments. *Elife*. **8**, e46923 (2019).
5. N. Lalam, Estimation of the reaction efficiency in polymerase chain reaction. *Journal of theoretical biology*. **242**, 947–953 (2006).
6. G. B. Gloor, J. M. Macklaim, V. Pawlowsky-Glahn, J. J. Egozcue, Microbiome datasets are compositional: And this is not optional. *Frontiers in microbiology*. **8**, 2224 (2017).
7. J. J. Egozcue, J. Graffelman, M. I. Ortego, V. Pawlowsky-Glahn, Some thoughts on counts in sequencing studies. *NAR Genomics and Bioinformatics*. **2**, lqaa094 (2020).
8. N. D. Gallo, E. Drenkard, A. R. Thompson, E. D. Weber, D. Wilson-Vandenberg, S. McClatchie, J. A. Koslow, B. X. Semmens, Bridging from monitoring to solutions-based thinking: Lessons from CalCOFI for understanding and adapting to marine climate change impacts. *Frontiers in Marine Science*. **6**, 695 (2019).
9. N. Hobbs, M. Hooten, *Bayesian models: A statistical primer for ecologists*. 593 princeton university press (Princeton, 2015).
10. J. D. Silverman, K. Roche, S. Mukherjee, L. A. David, Naught all zeros in sequence count data are the same. *Computational and structural biotechnology journal*. **18**, 2789–2798 (2020).
11. Stan Development Team, RStan: The R interface to Stan (2021), (available at <https://mc-stan.org/>).